

# We are IntechOpen, the world's leading publisher of Open Access books Built by scientists, for scientists

**4,800**

Open access books available

**122,000**

International authors and editors

**135M**

Downloads

Our authors are among the

**154**

Countries delivered to

**TOP 1%**

most cited scientists

**12.2%**

Contributors from top 500 universities



**WEB OF SCIENCE™**

Selection of our books indexed in the Book Citation Index  
in Web of Science™ Core Collection (BKCI)

Interested in publishing with us?  
Contact [book.department@intechopen.com](mailto:book.department@intechopen.com)

Numbers displayed above are based on latest data collected.

For more information visit [www.intechopen.com](http://www.intechopen.com)



# Synthesis, Surface Modification and Characterisation of Nanoparticles

L.S. Wang<sup>1</sup> and R.Y. Hong<sup>1,2,\*</sup>

<sup>1</sup>College of Chemistry, Chemical Engineering and Materials Science & Key Laboratory of Organic Synthesis of Jiangsu Province, Soochow University, SIP,

<sup>2</sup>College of Chemistry and Chemical Engineering, Fuzhou University, China

## 1. Introduction

Nanoparticles with sizes ranging between objects and microparticles (e.g. atom) have attracted much attention. These particles with various specialized functions not only deepen our understanding of nature, but also serve as the basis for the development of new advanced technology.

The successful application of nanoparticles depends upon both the synthesis and the surface modification of these particles. Surface modification can improve the inherent characteristics of the nanoparticles and serve to prepare nanocomposites inexistent in nature.

Nanocomposites are made from two or more of the solid phase, at least in one dimensional nano-level size (1-100 nm). The solid phase can be amorphous, semi-crystalline, grain, or a combination. The solid phase can also be organic, inorganic, or a combination. According to the size of the solid phase, nanocomposites generally include the following three types: nanoparticles and nanoparticle compounds (0-0 composite), nanoparticles and conventional bulk composites (0-3 composite) and composite nano-films (0-2 composite). In addition, the nano-layered structure material is ascribed to nano-material, and the multi-layer nanocomposite composed of different materials is also known as nanocomposites.

Composite materials own excellent performance, which can be widely used in aerospace, defense, transportation, sports and other fields. Nanocomposites are one of the most attractive part of the composite materials. Due to the fast development in recent years, nanocomposites are put in an important position by the developed countries in the development of new materials. The research on nanocomposites includes organic-inorganic composites, nano-polymer matrix composites and inorganic-inorganic composites. In this chapter, combined with our research experience, we mainly introduce the nano-polymer matrix composites to the readers. In order to claim the nano-polymer matrix composites exactly, synthesis and modification of nanoparticles and preparation, characterization and applications of nano-polymer matrix composites were mainly discussed.

## 2. Synthesis and modification of nanoparticles

### 2.1 Synthesis of nanoparticles

Nanoparticles are solids particles at the intermediate state, that is between atoms/molecules and macroscopic objects. Owing small size effect, large surface effect and quantum tunnel

effect, the nanoparticles demonstrate special physical properties and can be widely used in high density magnetic recording, radar signal absorbing, magnetic fluid, radio wave shielding, precision polishing, optical devices, thermal conducting gel for micro chips, electronic packaging, optoelectronics, high-performance battery, solar cell, efficient catalyst, efficient fire retardant, sensitive components, high-toughness ceramics, the body repairing, cancer therapy, and so on. Preparation of nanoparticles is an important branch of the materials science and engineering. The study of nanoparticles relates various scientific fields, e.g., chemistry, physics, optics, electronics, magnetism and mechanism of materials. Some nanoparticles have already reached practical stage. In order to meet the nanotechnology and nano-materials development in the next century, it is necessary to review the preparation techniques of nanoparticles.

Methods for preparation of nanoparticles can be divided into physical and chemical methods based on whether there exist chemical reactions. On the other hand, these methods can be classified into gas phase, liquid phase and solid phase methods based on the state of the reaction system. The gas phase method includes gas-phase evaporation method (resistance heating, high frequency induction heating, plasma heating, electron beam heating, laser heating, electric heating evaporation method, vacuum deposition on the surface of flowing oil and exploding wire method), chemical vapor reaction (heating heat pipe gas reaction, laser induced chemical vapor reaction, plasma enhanced chemical vapor reaction), chemical vapor condensation and sputtering method. Liquid phase method for synthesizing nanoparticles mainly includes precipitation, hydrolysis, spray, solvent thermal method (high temperature and high pressure), solvent evaporation pyrolysis, oxidation reduction (room pressure), emulsion, radiation chemical synthesis and sol-gel processing. Solid phase method includes thermal decomposition, solid state reaction, spark discharge, stripping and milling method.

We have synthesized several nanoparticles in our laboratory, such as:  $\text{TiO}_2$ ,  $\text{Fe}_3\text{O}_4$ ,  $\text{ZnO}$ ,  $\text{SiO}_2$  and YIG nanoparticles.

### 2.1.1 Synthesis of titania nanoparticles

Using titanium tetrachloride ( $\text{TiCl}_4$ ) as a precursor [1], titania nanoparticles were synthesized in the diffusion flame (DF) of air and liquid petrol gas (LPG). The effects of air and LPG flow rates and flow ratio, flame temperature and flame shape on the synthesized  $\text{TiO}_2$  nanoparticles were investigated. Experimental investigation, performed using the apparatus in Fig. 1, showed that the mean particle size of  $\text{TiO}_2$  increased obviously with

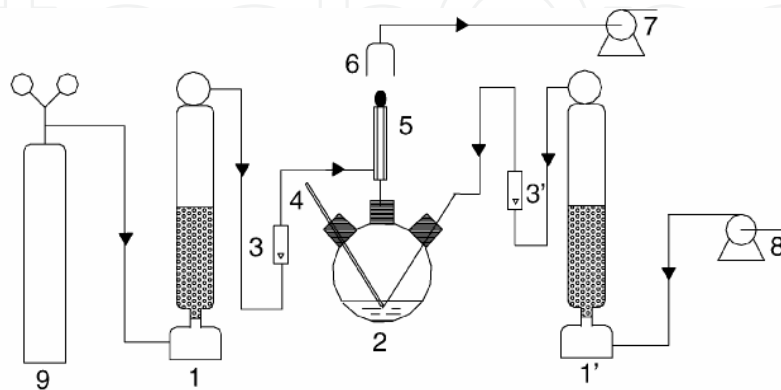


Fig. 1. Experimental flow diagram for synthesizing  $\text{TiO}_2$  nanoparticles using LPG/air flame. (1 and 1': Dryer, 2:  $\text{TiCl}_4$  evaporator, 3 and 3': rotameters, 4: thermometer, 5: combustor, 6: filter, 7: circulating-water vacuum pump, 8: air compressor, 9: LPG cylinder) [1].

increasing airflow rate, and not obviously with that of LPG, the mean particle size at optimal experimental condition was less than 20 nm, the rutile fraction in the synthesized powder increased with increasing flame temperature and the particle size was affected by the flame height. A particle-dynamic model, describing the nucleation and coagulation of titania monomers/nanoparticles, was used to account for the experimental results based on the isothermal assumption. Generally speaking, the calculated particle sizes from the particle dynamics were consistent with the experimental measurements, especially, when the feed concentration of  $\text{TiCl}_4$  was low.

### 2.1.2 Microwave synthesis of magnetic $\text{Fe}_3\text{O}_4$ nanoparticles

Magnetic ( $\text{Fe}_3\text{O}_4$ ) nanoparticles were prepared by the co-precipitation of  $\text{Fe}^{3+}$  and  $\text{Fe}^{2+}$ ,  $\text{NH}_3 \cdot \text{H}_2\text{O}$  [2] was used as the precipitating agent to adjust the pH of the suspension, and the aging of  $\text{Fe}_3\text{O}_4$  magnetic nanoparticles was accelerated by microwave (MW) irradiation [3]. The obtained  $\text{Fe}_3\text{O}_4$  magnetic nanoparticles were characterized by Fourier-transform infrared spectroscopy (FT-IR), transmission electron microscopy (TEM), X-ray diffraction (XRD) and vibrating sample magnetometer (VSM).

The average size of  $\text{Fe}_3\text{O}_4$  crystallites was found to be around 8-9 nm. Aged under MW irradiation,  $\text{Fe}_3\text{O}_4$  nanoparticles have more complete crystalline structure than those aged for 7 days at room temperature. The obtained nanoparticles are well indexed to the inverse cubic spinel phase of  $\text{Fe}_3\text{O}_4$ . In addition, it can be seen from Fig. 2 that  $\text{Fe}_3\text{O}_4$  nanoparticles aged under MW irradiation have a higher saturation magnetization than those aged for 7 days at room temperature, which is due to the well crystallinity of  $\text{Fe}_3\text{O}_4$  nanoparticles. Compared to  $\text{Fe}_3\text{O}_4$  nanoparticles aged for 7 days, the coercivity of samples aged under MW irradiation increased, which could be ascribed to the reduction of particle size of  $\text{Fe}_3\text{O}_4$ .

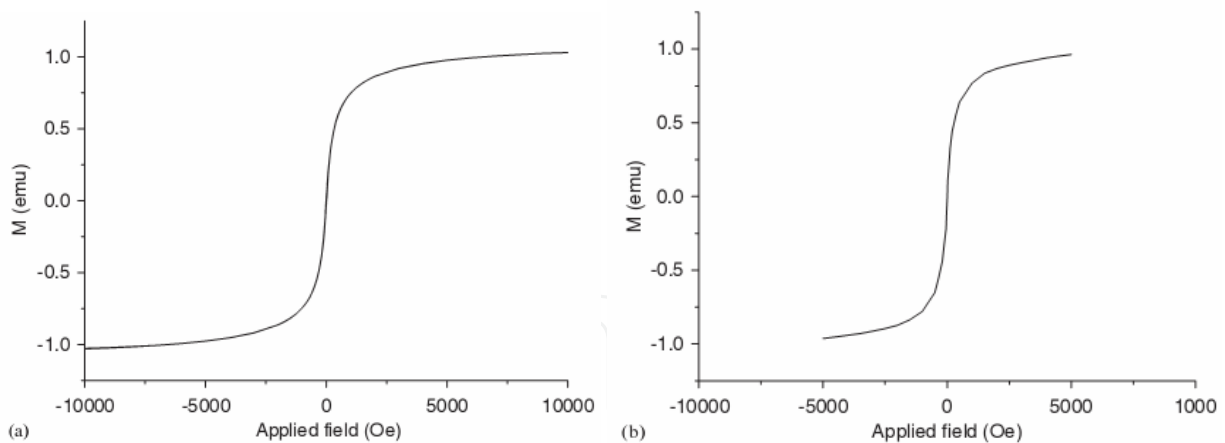


Fig. 2. Magnetic hysteresis curves of  $\text{Fe}_3\text{O}_4$  nanoparticles (sample A was aged under MW irradiation (a) and sample B was aged for 7 days at room temperature (b), respectively) [2].

### 2.1.3 Magnetic field synthesis of $\text{Fe}_3\text{O}_4$ nanoparticles

$\text{Fe}_3\text{O}_4$  nanoparticles were prepared by co-precipitation, and the aging of nanoparticles was improved by an applied magnetic field [4]. The obtained nanoparticles were characterized by FT-IR, scanning electron microscopy (SEM), XRD, and VSM. The results show that synthesized under an applied magnetic field, the aging time could be greatly reduced and the magnetic properties of  $\text{Fe}_3\text{O}_4$  nanoparticles could be improved.

### 2.1.4 Synthesis of Fe<sub>3</sub>O<sub>4</sub> nanoparticles without inert gas protection

Fe<sub>3</sub>O<sub>4</sub> nanoparticles were hydrothermally synthesized under continuous MW irradiation from FeCl<sub>3</sub>·6H<sub>2</sub>O and FeSO<sub>4</sub>·7H<sub>2</sub>O aqueous solutions, using NH<sub>4</sub>OH as precipitating reagent and N<sub>2</sub>H<sub>4</sub>·H<sub>2</sub>O as oxidation-resistant reagent [5]. The results of XRD, FT-IR spectroscopy and SEM measurements showed that the synthesized Fe<sub>3</sub>O<sub>4</sub> nanoparticles had an average diameter of 10 nm. The magnetic properties of the Fe<sub>3</sub>O<sub>4</sub> nanoparticles were measured using a VSM, indicating that the nanoparticles possessed high saturation magnetization at room temperature, as shown in Fig. 3. The Fe<sub>3</sub>O<sub>4</sub> nanoparticles synthesized at the optimal ratio of Fe<sup>3+</sup>/Fe<sup>2+</sup> of about 1.75:1 exhibit a maximal saturation magnetization of 84.83 emu/g. Hydrazine plays double roles both as the precursor of precipitator and as the oxidation-resistant reagent in the reaction system. The saturation magnetization of Fe<sub>3</sub>O<sub>4</sub> nanoparticles synthesized with hydrazine was greatly improved.

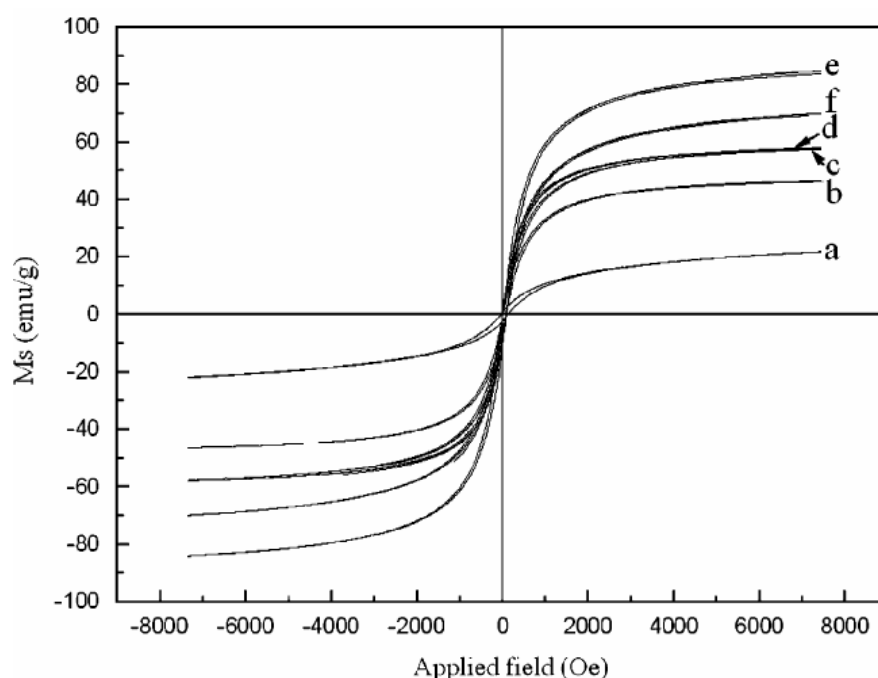


Fig. 3. (a) Hysteresis regress curve of Fe<sub>3</sub>O<sub>4</sub> nanoparticles synthesized using NaOH as precipitator at the ratio (Fe<sup>3+</sup>/Fe<sup>2+</sup>) of 1.75:1 without hydrazine. (b, f, e and d) Hysteresis regress curve of Fe<sub>3</sub>O<sub>4</sub> nanoparticles synthesized using NH<sub>4</sub>OH as precipitator at the ratio (Fe<sup>3+</sup>/Fe<sup>2+</sup>) of 1.25:1, 1.5:1, 1.75:1 and 2.0:1, respectively, with hydrazine. (c) Hysteresis regress curve of Fe<sub>3</sub>O<sub>4</sub> nanoparticles synthesized using NH<sub>4</sub>OH as precipitator at the ratio (Fe<sup>3+</sup>/Fe<sup>2+</sup>) of 1.5:1 without hydrazine [5].

### 2.1.5 Synthesis of ZnO nanoparticles by two different methods

ZnO precursor was synthesized by direct precipitation from zinc acetate and ammonium carbonate [6,7]. ZnO nanoparticles were obtained by calcination of the precursor at 450°C for 3 h and the calcination after the heterogeneous azeotropic distillation of the precursor, respectively. The synthesized ZnO nanoparticles were characterized by FT-IR, XRD and TEM. It is concluded that the heterogeneous azeotropic distillation of the precursor effectively reduced the formation of hard agglomerates, moreover, the photocatalytic activity of the synthesized ZnO nanoparticles is high.

### 2.1.6 Synthesis of silica powders by pressured carbonation

A method was proposed for the preparation of silica powders using inexpensive material of sodium silicate ( $\text{Na}_2\text{SiO}_3$ ) and carbon dioxide ( $\text{CO}_2$ ) by pressured carbonation, in which carbon dioxide acted as a precipitating reagent [8]. The flow sheet diagram is shown in Fig. 4.

Microstructure and size analyses of the precipitated silica powders were carried out using TEM and dynamic light scattering. The average particle size, size distribution and yield of silica powders were affected by reaction time, temperature and concentrations of surfactant and sodium silicate solutions. The particle size of silica powders increased with reaction temperature and concentration of sodium silicate, and the yield of silica powders increased with increasing reaction time, as shown in Table 1. The size distribution of silica powders was affected by concentration of surfactant PEG. The optimal preparation conditions were experimentally determined for obtaining the silica powders with nanometer size, narrow size distribution, spherical shape and high purity without sodium carbonate and surfactant.

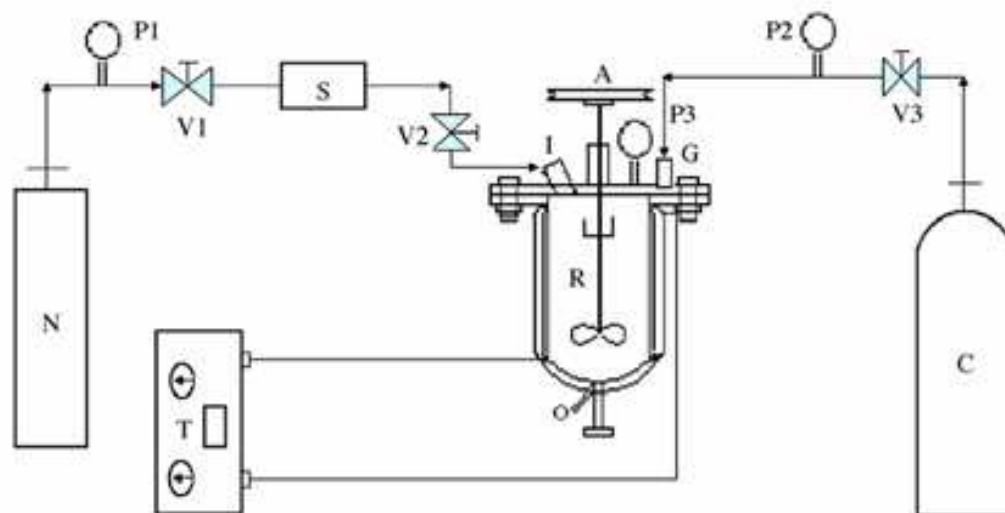


Fig. 4. Apparatus for the formation of ultrafine silica powders using carbon dioxide. (R, high-pressure reactor; C, carbon dioxide cylinders; T, temperature controller; I, solution inlet; O, product outlet; G, gas inlet; A, agitator; P1, P2 and P3, pressure gauges; V1, V2 and V3, control valves; S, solution injection device) [8].

No.	Temperature /°C	$\text{Na}_2\text{SiO}_3/\text{mol L}^{-1}$	PEG/%	Reaction time/h	Average size/nm	Yield/%
1	80	1.0	5.0	3	54	86.4
2	70	1.0	10	2	52	84.5
3	60	1.0	15	1	46	75.2
4	80	0.50	15	2	36	84.7
5	70	0.50	5.0	1	33	82.3
6	60	0.50	10	3	36	88.6
7	80	0.25	10	1	19	85.3
8	70	0.25	15	3	17	86.3
9	60	0.25	5.0	2	15	86.8

Table 1. Effect of temperature, content of  $\text{Na}_2\text{SiO}_3$  and PEG, reaction time on the yield and average size of silica [8].

### 2.1.7 MW-assisted synthesis of Bi-substituted yttrium garnet nanoparticles

Bi-substituted yttrium garnet (Bi-YIG,  $\text{Bi}_{1.8}\text{Y}_{1.2}\text{Fe}_5\text{O}_{12}$ ) nanoparticles were prepared by MW-assisted co-precipitation as well as conventional co-precipitation using ammonia aqueous solution as precipitant [9, 10]. The nanoparticles were characterized by thermal gravity-differential thermal analysis, XRD, TEM, dynamic light scattering, VSM and Faraday rotation meter, respectively. Results demonstrate that the Bi-YIG nanoparticles prepared by MW-assisted co-precipitation have smaller particle size, high saturation magnetization (see Fig. 5) and higher Faraday rotation than those prepared by the conventional co-precipitation.

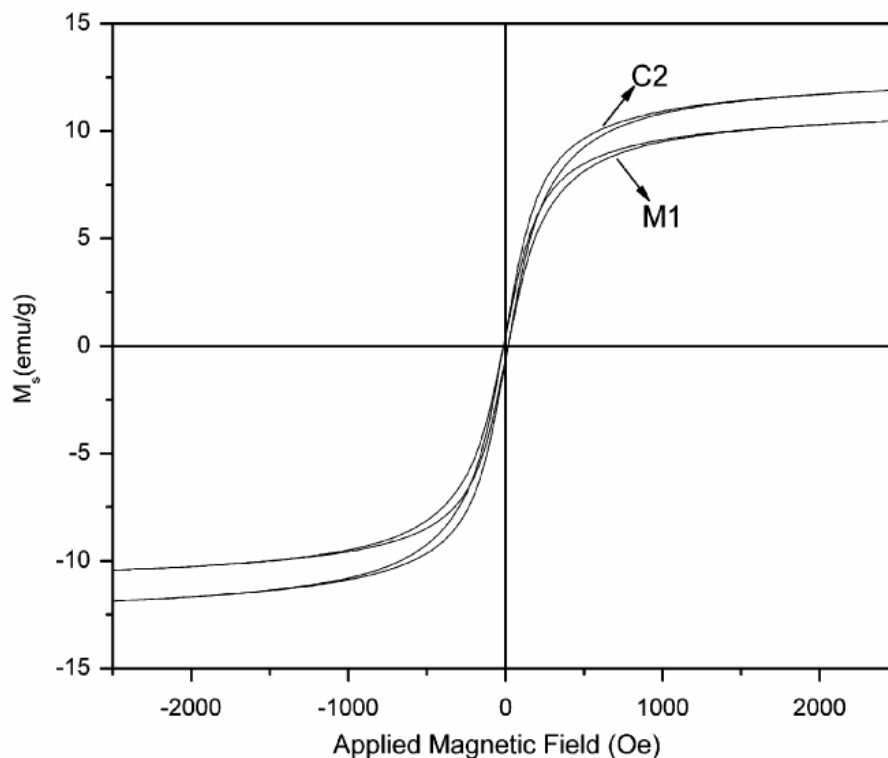


Fig. 5. Magnetic hysteresis of Bi-YIG particles: (M1) prepared by MW co-precipitation and (C2) prepared by conventional co-precipitation [9].

### 2.1.8 Molten-salt synthesis of Bi-substituted yttrium garnet nanoparticles

Compared to the MW-assisted method [11], Bi-YIG nanoparticles were successfully synthesized by molten-salt method in NaCl-KCl flux at 650°C. XRD, SEM, dynamic light scattering, VSM and Faraday rotation meter were used to characterize the phase, morphology, size distribution, magnetic properties and Faraday rotation of the as-prepared Bi-YIG nanoparticles, respectively. Results show that the average size of Bi-YIG nanoparticles prepared by molten-salt method is about 50 nm. The formation of Bi-YIG in molten-salt process was associated with the type of the raw material used. One can obtain pure Bi-YIG nanoparticles using oxides mixture, but can not obtain pure Bi-YIG nanoparticles using Bi-YIG precursors. The Bi-YIG nanoparticles began to form at 600°C and accomplished at 650°C, and one can obtain pure Bi-YIG phase at the temperature range of 650-800°C using molten-salt method.

## 2.2 Modification of nanoparticles

To improve or change the dispersion of the nanoparticles, and the compatibility between the nanoparticles and other materials, physical or chemical methods are needed to alter the physical, chemical, mechanical properties, and the surface structure of nanoparticles.

In order to control the surface of nanoparticles and to apply those nanoparticles in industry and biomedicine, in-depth understanding of the basic properties of the nanoparticles are indispensable.

According to the principles of surface modification, the surface modification of nanoparticles can be divided into partial chemical modification, mechanical and chemical modification, external membrane modification (ie, capsule), high-energy surface modification, surface modification using precipitation, esterification, coupling and grafting reactions. Surface modification in general is through physical adsorption coating or grafting depends on the properties of the particle surface. The use of ultraviolet ray for the plasma surface modification of particles belong to the physical modification. By the chemical reactions between the nanoparticle surface and modifier, the surface structure and state of nanoparticles are changed. Surface chemical modification of nanoparticles plays a very important role to reduce the agglomeration. Due to modifier adsorption or bonding on the particle surface, which reduces the surface force of hydroxyl groups, the hydrogen bonds between particles are eliminated to prevent the formation of oxygen bridge bonds when nanoparticles are drying, thereby preventing the occurrence of agglomeration.

### 2.2.1 Surface modification of ZnO nanoparticles

ZnO nanoparticles were synthesized by homogeneous precipitation. To reduce the aggregation among ZnO nanoparticles, an effective surface modification method was proposed by grafting polymethyl methacrylate (PMMA) onto the ZnO particles [12]. That is, the surface of ZnO nanoparticles was firstly treated with a KH570 silane coupling agent, which introduces functional double bonds onto the surface of ZnO nanoparticles, followed by radical grafting polymerization in non-aqueous medium. The obtained nanocomposite was characterized by FT-IR, TG, sedimentation test, SEM, and XRD. The results of FT-IR and TG showed that the desired polymer chains have been covalently bonded to the surface of ZnO nanoparticles. It was found that the increasing monomer concentration could increase the grafting percentage and hence promote the dispersibility.

To reduce the aggregation among nanoparticles and to improve the compatibility between nanoparticles and the organic matrix, poly(styrene) (PS) was grafted on to the ZnO nanoparticles in a non-aqueous suspension. The test shows that bare ZnO nanoparticles have high photocatalytic activity, while PS-grafted ZnO composites have almost no photocatalytic activity. Surface modification by grafting polymerization can reduce the aggregation of nanoparticles and help to form a stable suspension in organic solvents.

### 2.2.2 Surface modification of Fe<sub>3</sub>O<sub>4</sub> nanoparticles

In order to prepare stable magnetic fluid, the surface of Fe<sub>3</sub>O<sub>4</sub> nanoparticles was modified with different surfactants in our research [13,14].

Using two kinds of surfactants, stable water-based magnetic fluid was prepared. The surface of Fe<sub>3</sub>O<sub>4</sub> nanoparticles was coated with oleate sodium as the primary layer and polyethylene glycol 4000 (PEG-4000) as the secondary layer to improve the stability of water-based magnetic fluid [15]. The dosages of oleate sodium and PEG-4000 were found to have an



important effect on increasing the solid content. Gouy magnetic balance showed that the saturation magnetization could be as high as  $1.44 \times 10^5$  A/m.

To prepare a biocompatible water-based magnetic fluid, the  $\text{Fe}_3\text{O}_4$  nanoparticles were modified by dextran through a two-step method [16]. The  $\text{Fe}_3\text{O}_4$  nanoparticles were first surface modified by amino-silane, and then coated by dextran. The influences of dextran molecular weight on the size, morphology, coating efficiency and magnetic property of magnetite/dextran nanocomposite were investigated. The magnetite/dextran nanocomposite was dispersed in water to form a magnetic fluid by ball milling. The molecular weight of dextran plays an important role on the size, morphology, coating efficiency, and magnetic property of magnetite/dextran nanocomposite. The surface modification of  $\text{Fe}_3\text{O}_4$  nanoparticles with dextran is propitious to the stability of magnetic fluid. The viscosity of magnetic fluid increases with the increasing molecular weight of dextran. An external magnetic field can enhance the interaction among magnetic fluid, therefore, the viscosity of magnetic fluid increases under the external magnetic field. The magnetic field could also rearrange the  $\text{Fe}_3\text{O}_4$  nanoparticles, leading to the formation of orderly microstructures. When there is no magnetic field, the viscosity of magnetic fluid increases linearly with the solid content. If an external magnetic field is applied, the viscosity increases quadratically with the solid content. Then, the dextran stabilized magnetic fluid were used to perform the MRI experiments on the living rabbits with VX2 malignant tumor, the results showed that these nanoparticles appear to be a promising vehicle for MR imaging [17].

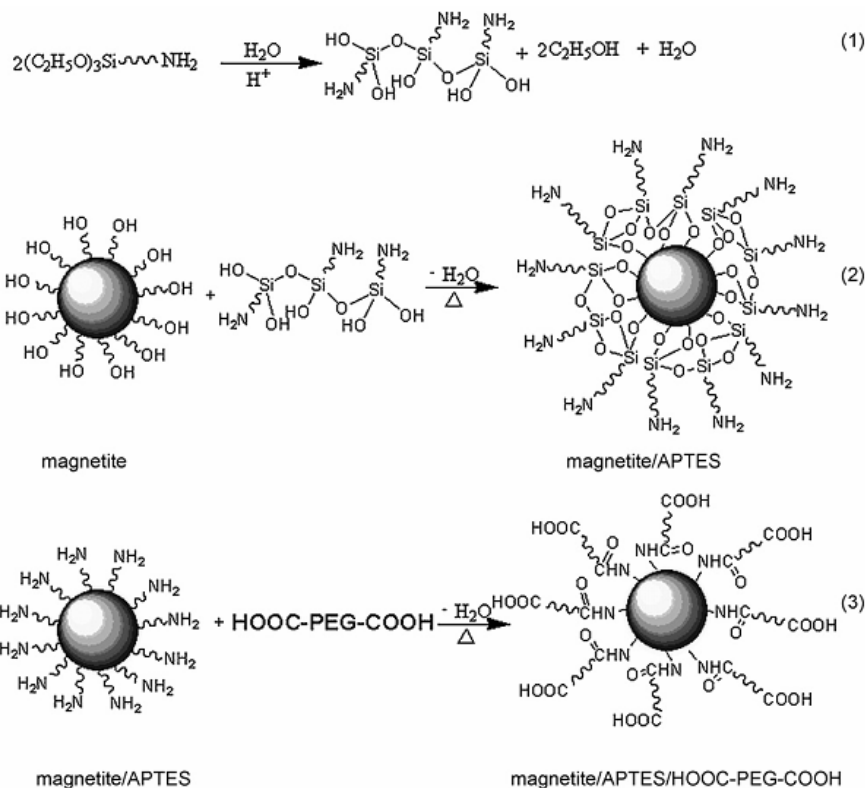


Fig. 6. Synthesis route for the PEG diacid coated magnetite nanoparticles: (1) simplified reaction of hydrolysis and condensation with production of silane polymer; (2) scheme of the simplified silanization reaction of APTES on the magnetite surface; (3) simplified reaction of HOOC-PEG-COOH on the magnetite surface after treated by APTES [17].

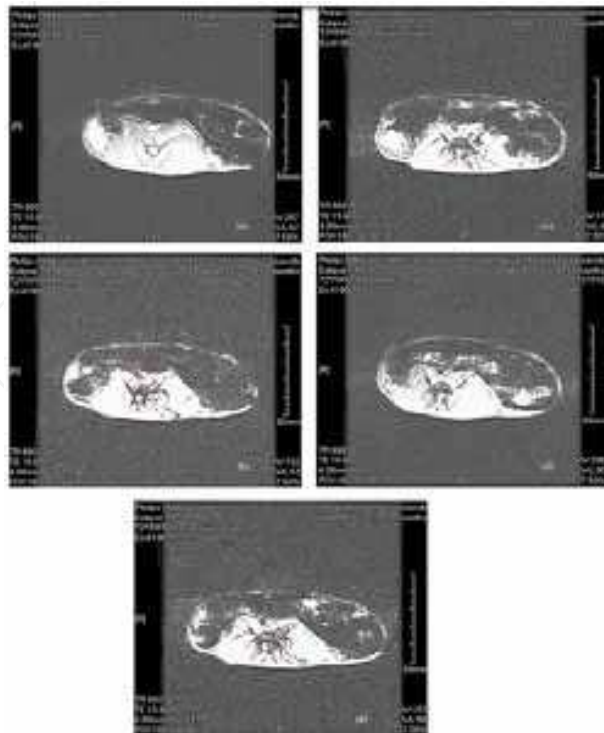


Fig. 7. T2-weighted MR images acquired before (a) and at different times after the injection of magnetic fluid (b: 30 min, c: 60 min, d: 90 min, e: 120 min) [17].

In addition, we prepared kerosene-based magnetic fluid via a simple one step phase-transfer method [18]. The  $\text{Fe}_3\text{O}_4$  nanoparticles formed in the aqueous phase firstly modified by oleic acid and then migrated to the organic phase of kerosene to form a magnetic fluid. The size of  $\text{Fe}_3\text{O}_4$  nanoparticles was found to be around 10 nm by TEM. The magnetic fluid demonstrated superior stability, and had susceptibility of  $7.78 \times 10^{-4}$  and saturation magnetization of 27.3 emu/g. The rheological property [19] of the prepared magnetic fluid was investigated using a rotating rheometer attached with a custom-built solenoid coil. It was found that the viscosity of the magnetic fluid increased with the increasing intensity of magnetic field, and the magnetic fluid demonstrated shear-thinning behavior and could be described by the Herschel-Bulkey model.

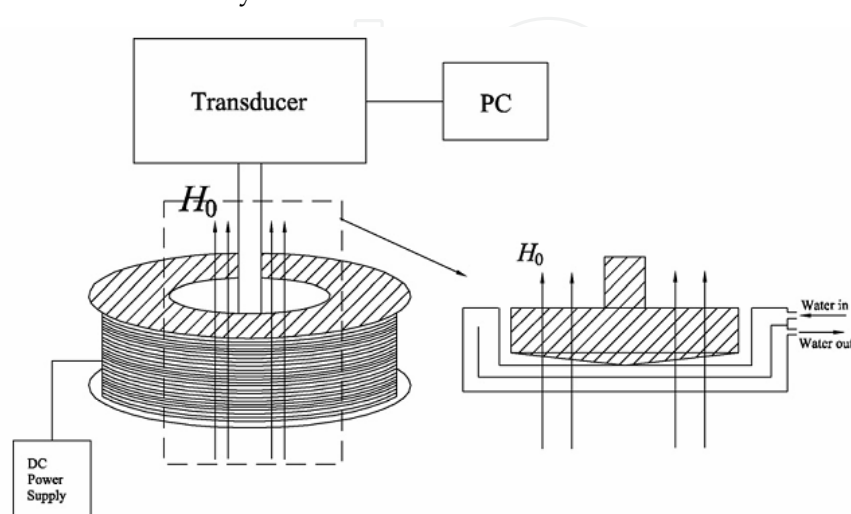


Fig. 8. A rotating rheometer for measuring viscosity under applied magnetic field [18].

### 2.2.3 Surface modification of silica nanoparticles

To prepare excellent silica reinforced PMMA [14,20], we first modified the silica with silane coupling agent (g-methacryloxypropyl trimethoxy silane, KH570), followed by in situ bulk polymerization. The modified silica nanoparticles were characterized by FT-IR, TEM and TG. Sedimentation tests and lipophilic degree (LD) measurements were also performed to observe the compatibility between the modified silica nanoparticles and organic solvents. The resultant polymers were characterized by UV-vis, Sclerometer, differential scanning calorimetry (DSC). The mechanical properties of the hybrid materials were measured. The results showed that the glass transition temperature, surface hardness, flexural strength as well as impact strength of the silica-nanoparticle reinforced PMMA slices were improved. Moreover, the tensile properties of PMMA films doped with silica nanoparticles via solution blending were enhanced.

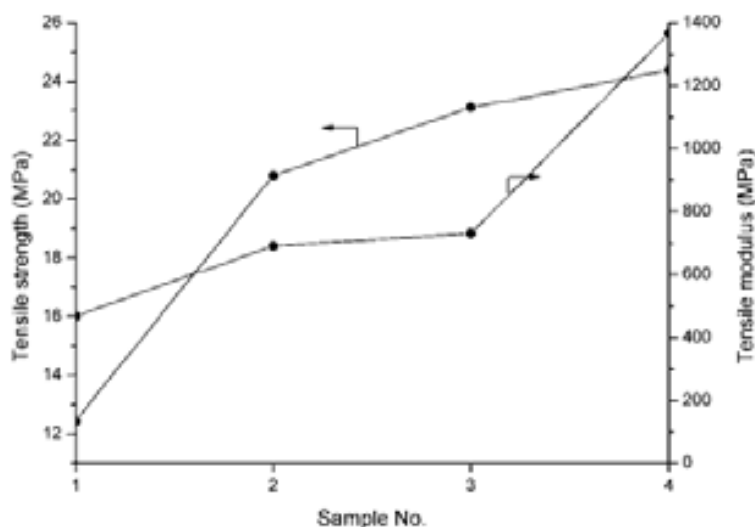


Fig. 9. Effects of silica nanoparticles on the properties of PMMA films. 1: neat PMMA, 2: unmodified silica+PMMA, 3: KH570-grafted silica+PMMA, 4: PMMA-grafted silica+PMMA [20].

## 3. Preparation and characterization of polymer-inorganic nanocomposites

### 3.1 Nano-polymer matrix composites

Since the sixties of the 20<sup>th</sup> century, P.J. Flory began to study the chain structure of polymer in solution. He thought that the polymer structure can be divided into three levels. One is chain structure, such as polyethylene; the second is conformation structure, such as isotactic polypropylene and syndiotactic polypropylene; the last is condensed state, such as liquid crystal polycarbonate, semi-crystalline polyether ether ketone, and so on. After different researches, researchers have proposed several models for the polymers possessing secondary or tertiary structure, as shown in Fig. 10.

Polymer possessed condensed state mainly refers to crystalline state, and the crystalline spherulites form is shown in Fig. 11. The condensed state can be divided into four phases, namely: no fixed shape, the transition state, liquid crystal state and crystalline state. Ascribing to the complex formation process and peculiar phenomenon, transition state and liquid crystal state have attracted much attention. The crystalline state is interesting mainly due to its multi-crystalline form.

**Secondary structure**

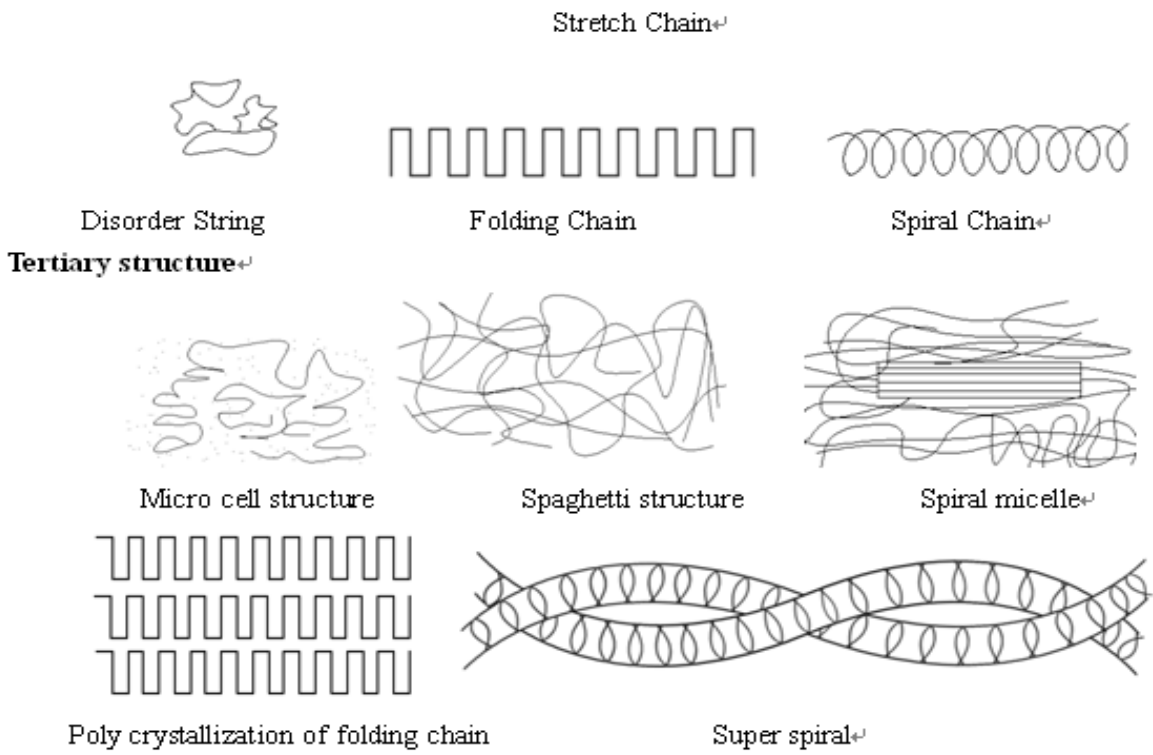


Fig. 10. Several models for the polymers possessing secondary or tertiary structure.

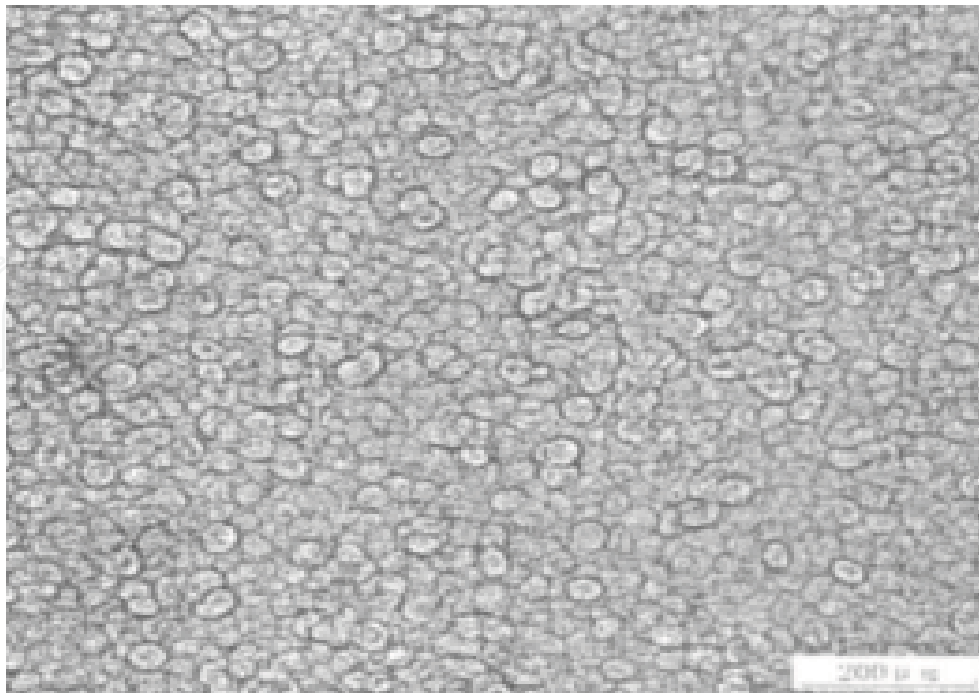


Fig. 11. Crystalline spherulites form of polypropylene under polarizing microscope [21]

Nano-composite material is the combination of the nano-sized powders and the the polymer matrix. In such materials, organic polymer generally is a continuous phase, and the nanoparticles the dispersed phase, such as,  $\text{BiI}_3$ -nylon11 nanocomposites and nylon-montmorillonite nanocomposites. In the new century, the rapid development of nano-composite materials becomes one of the most advanced composite materials.

When the nanoparticles were introduced into organic polymer matrix, the polymorphic crystalline would be induced, giving the nano-polymer matrix composites many excellent properties. Advantages of the nano-polymer matrix composites mainly include: (1) the increased properties of polymers, such as higher heat distortion temperature, rapid crystallization, improved mechanical properties, etc.; (2) a resource-saving compound, using only the common raw materials, and no other new materials; (3) the original process route: nano-composite uses the original route of polymer processing. These features make the nanocomposites easier to produce industrially, once breakthrough was obtained. In other words, nano-polymer matrix composites can provide an epoch-making performance by adjusting the complex dispersion of the original materials.

Polymer-inorganic nanocomposites own the machinability of organic materials and the functional and structural properties of inorganic materials, becoming the hot spot of today's science and technology. In the nanocomposites, a large part of the nano-materials is functional. For example,  $\text{BiI}_3$ /nylon11 nanocomposites show X-ray induced conductivity, the nanoparticles in the PS-clay nanocomposites display liquid crystal inducing behavior, and  $\alpha$ -FeOOH is used as a nuclear assembly agent in polymer LB films, and so on. In addition, nano-materials provide directional characteristics, and its direction-related features, including the coupling characteristics, can be used in the design process. Since the presence of anisotropy and coupling characteristics, the direction and sequence can be designed and tailored, according to the mechanical characteristics and function. With the presence of a dual nature, nano-materials can be more evenly dispersed in the matrix by adjusting the interaction of the interface of the two roles. The intervention of nano-whiskers, nano-rods, nano-wires and nano-beam offers the possibility of the enhanced orientation and maintains the processing facilities of the filled nanoparticles. In the polymer-inorganic nanocomposites, different interfaces also create synergies. To maximize the beneficial effects and synergies of different interfaces of the nanocomposites, the surface modification or treatment is generally appropriated, which forms a link with the substrates (eg covalent, hydrogen bond, intermolecular force, etc.), maximizing the dispersion and the appropriate combination.

Generally, the inorganic materials used to prepare the nano-composites mainly include layered silicate clay, layered compounds, metal powder and a variety of inorganic oxides. In our researches, nano-sized zinc oxide, iron oxide, silica and YIG were synthesized and employed to prepare a variety of polymer nanocomposites, giving the composite materials many new features. The chapter based on our research discusses the methods of preparation and characterization of the polymer-inorganic nanocomposites.

### **3.2 Preparation of polymer-inorganic nanocomposites**

Many methods could be applied to prepare polymer-inorganic nanocomposites, such as sol-gel processing, in-situ polymerization, particle in-situ formation, blending, radiation synthesis, and so on.

#### **3.2.1 Sol-gel processing**

Sol-gel processing is the method that the metal alkoxide or inorganic salt, through solution, sol, gel, curing, and then heat treatment, become solid oxide or other compounds.

Organic/inorganic nanocomposites are usually prepared by sol-gel in the solvent containing precursors and organic polymers. The most direct way is that the precursors hydrolyzed and condensed at the presence of polymer in the solvent systems. If the condition was under control, the polymer would not occur in isolation during the formation and drying process, through which can obtain optical transparent composite materials. Materials prepared by sol-gel processing have uniformity, high purity and low sintering temperature than that by conventional solid state reaction. The biggest problem of sol-gel is that the gel process would lead to a considerable contraction of the internal stress which could result in contraction of brittle materials, due to the evaporation of solvents, small molecules, water. Moreover, this method requires polymers in sol-gel system be dissolved in the condensate. In addition, the precursors are expensive and sometimes toxic, preventing the further improvement and application.

### 3.2.2 In situ polymerization

This is a class of the simplest and most representative method for the preparation of composite materials. Generally, the inorganic precursor and organic monomer were firstly mixed together, and then water and catalyst were added for condensation of inorganic precursors. Subsequently, oxidant was added for in situ polymerization, and the obtained materials were dried, through which organic/inorganic nanocomposites were prepared. We prepared PMMA/silica nanocomposites by in situ bulk polymerization of a silicic acid sol and MMA mixture [22]. Silicic acid was prepared by hydrolysis and condensation of sodium silicate in the presence of 3.6 M HCl. Silicic acid sol was obtained by tetrahydrofuran (THF) extraction of silicic acid from water. Each set of PMMA/silica composites was subjected to thermal and mechanical studies. With increase in silica content, the PMMA/silica nanocomposites filled with silica particles showed improved thermal and mechanical properties, whereas a decrease in thermal stability.

### 3.2.3 Particle in situ formation

Polymers and inorganic hybrid precursors were dissolved in a suitable solvent, and the molecules of polymer and precursors combined together. Via a reaction, such as metal alkoxide hydrolysis, oxidation and reduction reactions, and so on, inorganic nanoparticles were in-situ formed in the polymer. Using the adsorption and complexation of metal ions of polymer-specific functional groups or the space constraints between polymer and reactant, nanocomposites were prepared in situ. The methods for generating nanoparticles can be radiation, heat, light, gas reactions, and so on. By this way, the obtained inorganic particle was usually nanometer size, and uniformly dispersed in polymer. Therefore, the compounds own a transparent stable structure. Moreover, the polymer plays a role of size controlling and aggregation preventing of inorganic nanoparticles. In our research, ultra-small magnetite nanoparticles were prepared using chitosan-polyacrylic acid (CS-PAA) nanospheres as template [23]. The CS-PAA hollow nanospheres could be prepared by polymerization of acrylic acid monomers in the presence of chitosan. The  $\text{Fe}_3\text{O}_4$  loading was done by dissolving  $\text{FeCl}_3 \cdot 6\text{H}_2\text{O}$  and  $\text{FeSO}_4 \cdot 7\text{H}_2\text{O}$  into CS-PAA nanospheres solution followed by adding  $\text{NH}_4\text{OH}$ . Finally, CS-PAA template could be removed by adjusting with HCl to  $\text{pH} < 1$ . The obtained particles were characterized by dynamic light scattering (DLS) in aqueous solution and observed by TEM, FT-IR and X-ray. The results revealed that the  $\text{Fe}_3\text{O}_4$  nanoparticles were 3-5 nm in size with excellent dispersibility. The particles exhibited superparamagnetic property with saturation magnetizations of 40.7 emu/g.

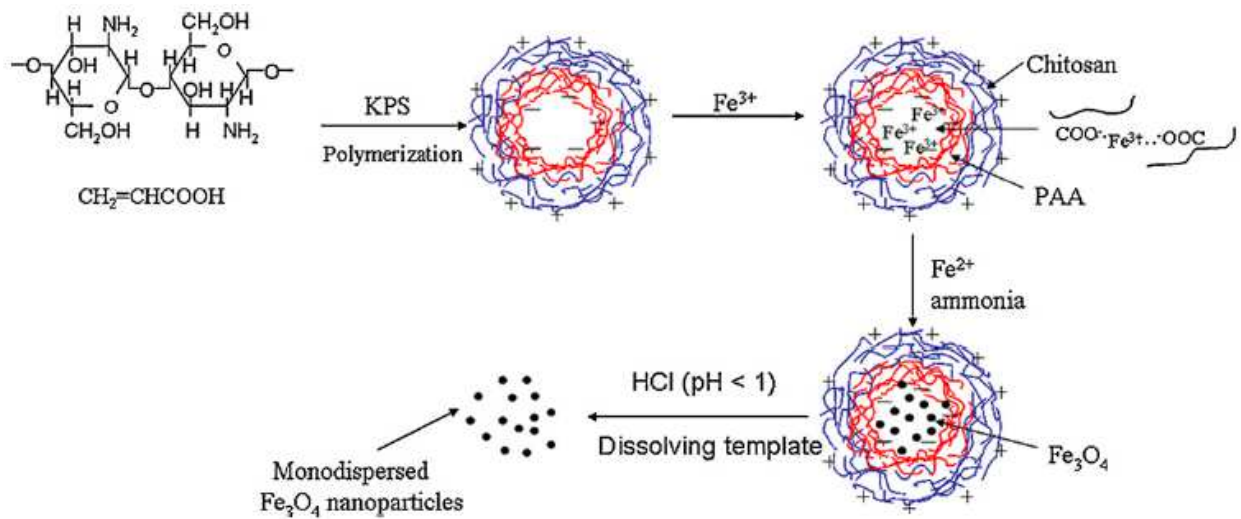


Fig. 12. The procedure for monodisperse magnetite nanoparticles via chitosan-poly(acrylic acid) template [23].

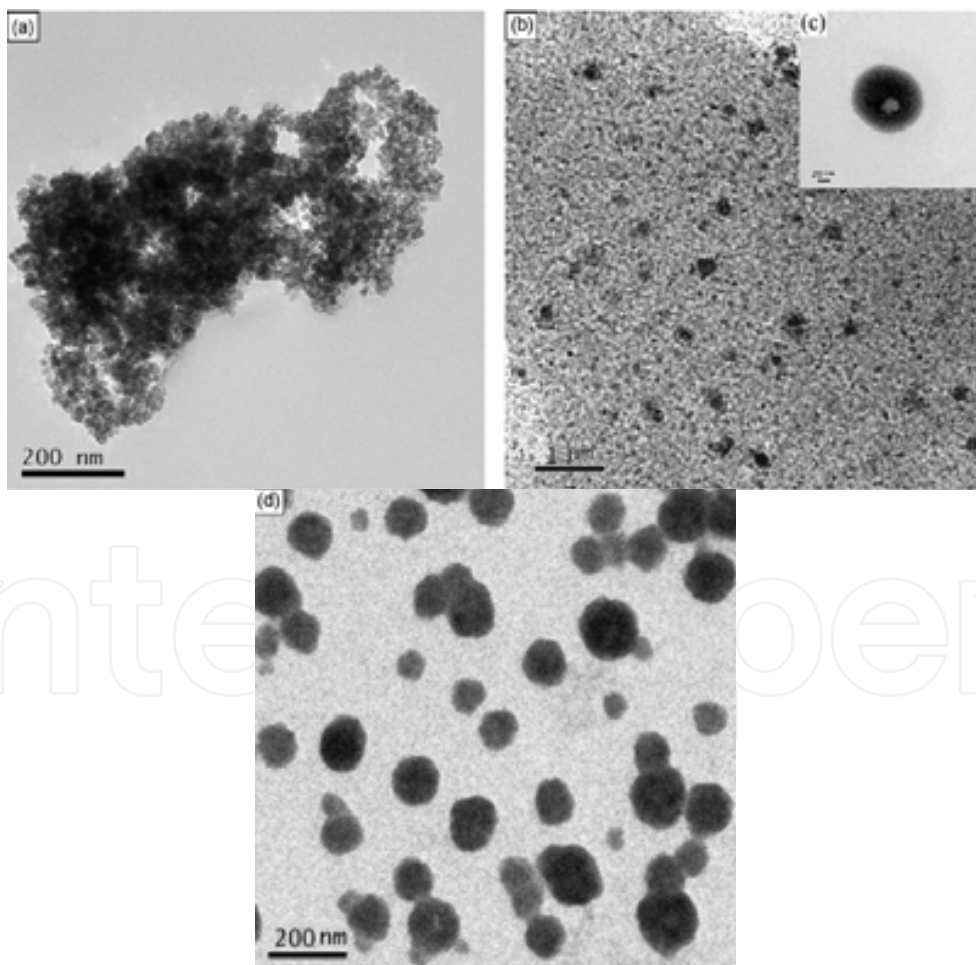


Fig. 13. TEM images of (a) bare  $\text{Fe}_3\text{O}_4$  nanoparticles; (b) CS-PAA particles; (c) magnified CS-PAA particles; (d)  $\text{Fe}_3\text{O}_4$  nanoparticles synthesized by CS-PAA template [23].

### 3.2.4 Blending

Blending is the simplest way to prepare nanocomposites, and is suitable for all kinds of nanoparticles. According to the conditions, blending usually can be divided to solution blending, emulsion or suspension blending and melt blending.

#### 3.2.4.1 Solution blending

Firstly, the nanoparticles were added after the base resin was dissolved in solvent. The obtained mixture was agitated to prepare a uniform mixture. The nanocomposites were prepared by removing the solvent or making polymerization of the monomer. In our research, polyurethane-based coatings reinforced by ZnO nanoparticles (about 27 nm) were prepared via solution blending [24]. The ZnO/PU films and coats were fabricated by a simple method of solution casting and evaporation. The mechanical properties of the films were investigated by a universal material test, and the abrasion resistance of the prepared coats was evaluated by a pencil-abrasion-resistance tester. It was found that significant improvement of the PU films in Young's modulus and tensile strength was achieved by incorporating ZnO nanoparticles up to 2.0 wt%, and that the abrasion resistance of the PU coats was greatly enhanced due to the addition of ZnO nanoparticles. Moreover, the antibacterial property test was carried out via the agar dilution method and the result indicated that PU films doped with ZnO nanoparticles showed excellent antibacterial activity, especially for *Escherichia coli*.

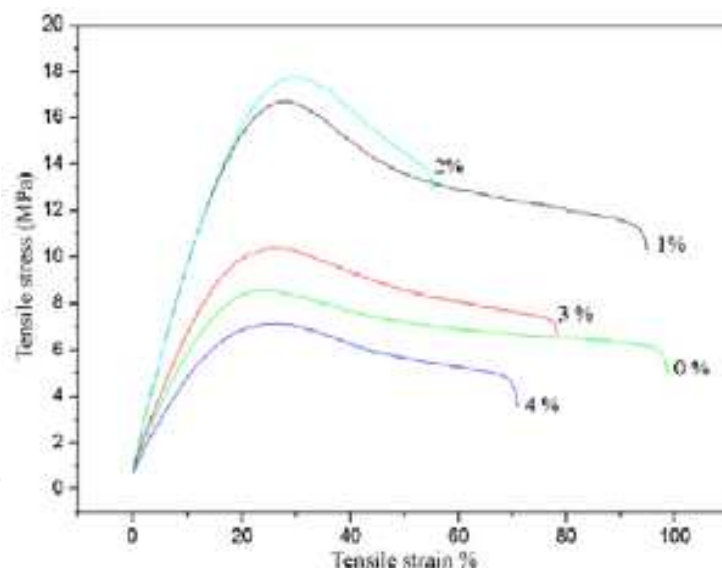


Fig. 14. Tensile stress-strain curves of different PU films [24].

ZnO(wt%)	Antibacterial rate	
	<i>Escherichia</i> (CPU)	<i>Bacillus subtilis</i> (CPU)
0	0	0
1.0	20	0
2.0	26	18
3.0	71	61
4.0	90	84

Table 2. Antibacterial rate of PU films containing different content of ZnO nanoparticles [24].



Besides, the  $\text{Bi}_x\text{Y}_{3-x}\text{Fe}_5\text{O}_{12}$  ( $x = 0, 1$  and  $1.8$ )-doped PMMA nanocomposites were prepared by in situ bulk polymerization [25]. Some  $\text{Bi}_x\text{Y}_{3-x}\text{Fe}_5\text{O}_{12}$  nanoparticles (0.05 wt%) were dispersed in MMA monomer, and the obtained suspension was mixed in a high-performance ball mill operating at 40 rpm for 4 h. Some AIBN (0.1 wt% of monomer) as initiator was added. The prepolymerization was performed at  $80 \pm 2^\circ\text{C}$  under mechanical stirring for about 20 min until the conversion of MMA was about 12-15%. Then, the suspension was poured into a stainless steel mold, which was coated with a thin film of Garry Mould Release Agent (non-paintable). The aperture at the top of the mold was wrapped with a plastic foil. Thereafter, the mold containing the prepolymer and  $\text{Bi}_x\text{Y}_{3-x}\text{Fe}_5\text{O}_{12}$  nanoparticles was kept at  $40^\circ\text{C}$  for 24 h, and the solidification took place. Then, the temperature was adjusted to  $100^\circ\text{C}$  and kept for 1 h to increase the molecular weight of PMMA. Finally,  $\text{Bi}_x\text{Y}_{3-x}\text{Fe}_5\text{O}_{12}$  ( $x = 0, 1$  and  $1.8$ )-doped PMMA nanocomposites were obtained after disassembling the molds. The PMMA slice doped with Bi-YIG nanoparticles is a new promising material for magneto-optical devices. The Faraday rotation test showed that the angle of Faraday rotation increased with increasing Bi content in PMMA composites, and the maximum figure of merit was  $1.46^\circ$ , which was comparable to the value of a sputtered film.

### 3.2.4.2 Emulsion or suspension blending

Similar to solution blending, emulsion or suspension solution was used instead of solution [26]. The method is mainly applicable to the case of polymer difficult to dissolve. Superparamagnetic magnetite/polystyrene composite particles were prepared by inverse emulsion polymerization with water-based magnetic fluid as dispersing phase and organic solvent and styrene as continuous phase. The resultant brownish  $\text{Fe}_3\text{O}_4/\text{PS}$  emulsion showed magnetism in an applied magnetic field. The obtained magnetic  $\text{Fe}_3\text{O}_4/\text{PS}$  microspheres were characterized by FT-IR, TEM, SEM, XRD and TG. The magnetic  $\text{Fe}_3\text{O}_4/\text{PS}$  microspheres with a diameter of 200 nm were observed. The results showed that magnetite particles were well encapsulated in PS and the composite particles have high magnetite contents, which was more than 15%.

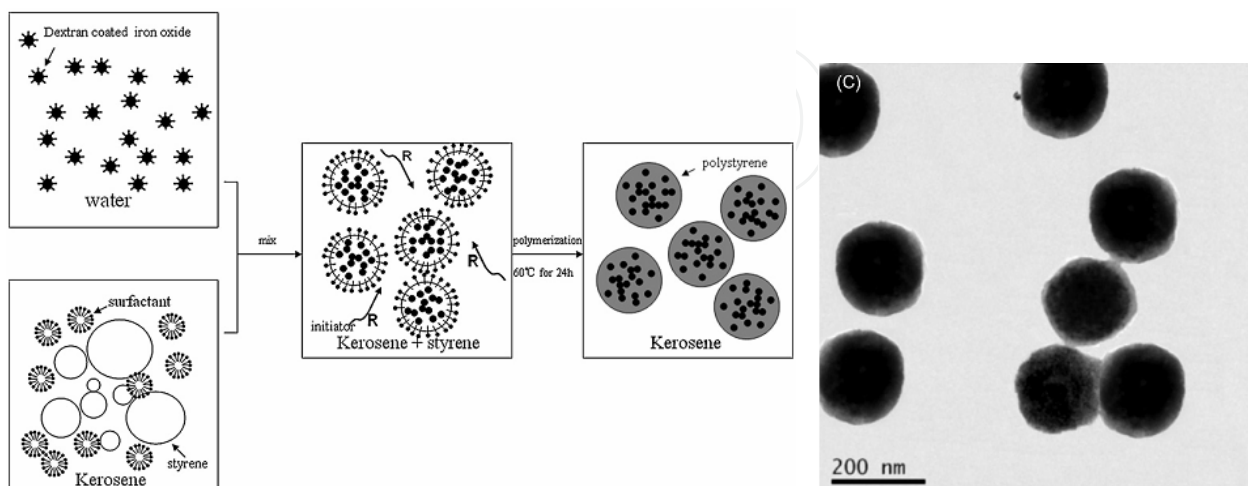


Fig. 15. The procedure for preparation of  $\text{Fe}_3\text{O}_4/\text{PS}$  composite particles by inverse emulsion polymerization (left); TEM images of  $\text{Fe}_3\text{O}_4/\text{PS}$  composite microspheres (right) [26].

### 3.2.4.3 Melt blending

To prevent aggregation, the surface of the nanoparticles was firstly modified with a suitable agent, and then the nanoparticles were added to the polymer in the molten state uniformly. Advantage of the method is similar to ordinary polymer modification, and is easy to industrialization. LDPE/EGP electrical conducting composites were prepared using low density polyethylene (LDPE) and expanded graphite (EGP) via melt blending [27]. The effects of EGP on the electrical and mechanical properties and Positive Temperature Coefficient (PTC) of the prepared composites were investigated. Results showed that the tensile strength of the composites decreased with the increasing content of EGP, and the EGP content should be lower than 40%. The PTC strength of the composites increases firstly and then decreases along with the increasing EGP content and achieved the maximum value of about 5.85 at 33% of filling content. Moreover, it was found that the PTC strength of the composites was affected by the heat treatment and blending time.

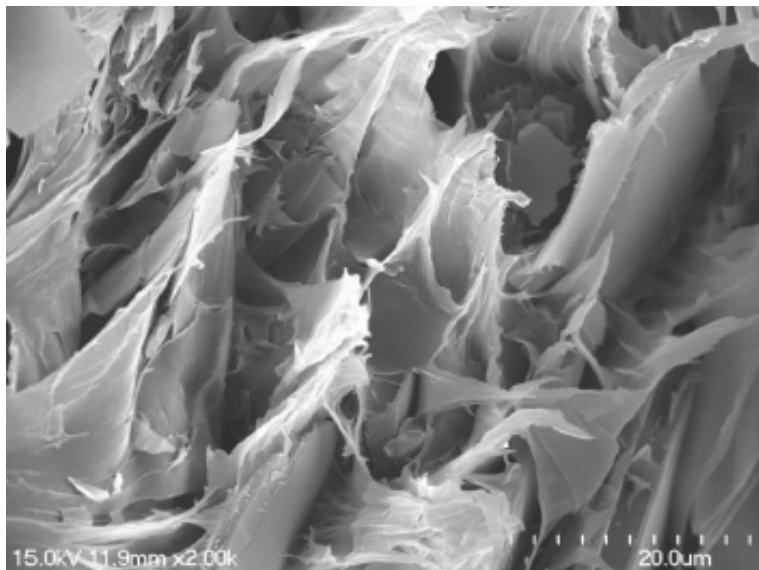


Fig. 16. SEM of the fracture of EGP/LDPE composites (35% EGP, no phase separation) [27].

### 3.2.4.4 Mechanical grinding blending

Using mechanical grinding blending, many kinds of magnetic fluids could be prepared. Firstly, polymer and some surfactants were dissolved in a solvent. Then, some magnetic nanoparticles were added and mixed together. The mixture was ball milled at 40 rpm for 3 h at room temperature using a high-performance ball mill under airtight condition. The pots and balls were made of agate. After ball milling for a suitable time, magnetic fluids were prepared.

### 3.2.5 Others

Recently, there are many reports on the use of special methods for preparing polymer/inorganic nanocomposites, such as MD and LB membrane method and radiation synthesis. In the LB membrane method, single or multilayer film is firstly pre-formed with metal ions, and then reacted to form sulfide nanoparticles. MD membrane method is the

way, using electrostatic interaction between cation and anion, to prepare single or multi-ordered membrane. Radiation synthesis is a recently developed method for the preparation of nanocomposites. Firstly, polymer monomer and metal salt mixed together at the molecular level, and then reacted under irradiation. The preparation method according to the system can be divided into two ways: the water system and the non-water system.

### 3.3 Characterization of polymer-inorganic nanocomposites

As we all know nanomaterials possess the following characters: small size and large specific surface area, high surface energy, a large proportion of surface atoms. As a result, one must have special "eye" and "hand" to characterize the nano-scale structure and properties of materials, and to effectively control its size, morphology, crystalline phase, composition and structure.

#### 3.3.1 X-ray diffraction

From the XRD data, one can obtain the material composition, structure (three-dimensional coordinates of atoms, chemical bonding, molecular conformation and three-dimensional conformation, the electron density value, etc.) and the information on the interaction between molecules. XRD is a common means of measuring nanoparticles. It can not only determine the sample phase and the phase content, but also the particle size. When the grain size is less than 100 nm, the diffraction line broadening will occur. The diffraction lines of the half-peak width of degree  $\beta$  department and crystal grain size ( $D$ ) has the following relationship:

$$\beta = 0.89\lambda / D \cos\theta$$

Accordingly, the strongest diffraction peak can be used to calculate the particle size of the prepared nanomaterials.

From X-ray photoelectron spectroscopy one can obtain the following information: (1) the element contents, except H and He from the fingerprint of the Eb (the binding energy of atoms in a particular orbit) spectrum. (2) the chemical valence state, chemical structure and physical state according to displacement of peak and the shape. (3) the semi-quantitative element analysis of chemical states from the relative intensity ratio of peak. (4) different elements, chemical state depth distribution and the film thickness from the peak and the change of the background intensity. In general, the higher Eb, the less electron density corresponding to the element is.

In our research, it was found that the magnetism of  $\text{Fe}_3\text{O}_4$  nanoparticles vanished at 550°C when exposed in the atmosphere for 2 h [28]. To find the reason of magnetism vanishment of pure  $\text{Fe}_3\text{O}_4$  nanoparticles, XRD was performed using Cu K $\alpha$  radiation. The XRD patterns of pure  $\text{Fe}_3\text{O}_4$  nanoparticles calcined at different temperatures are shown in Fig. 17. One can find from the that there is almost no difference among the diffraction peaks of the particles calcined at 150°C and 250°C except the weakening in intensity of magnetite, especially for (3 1 1) peak. From 350°C to 550°C, the (3 1 1) peak keeps reduction, while (1 0 4) peak of hematite develops and becomes increasingly stronger. The magnetite ( $\text{Fe}_3\text{O}_4$ ) transforms to hematite ( $\alpha\text{-Fe}_2\text{O}_3$ ) completely at 550°C, and the the magnetism of the nanoparticles vanished.

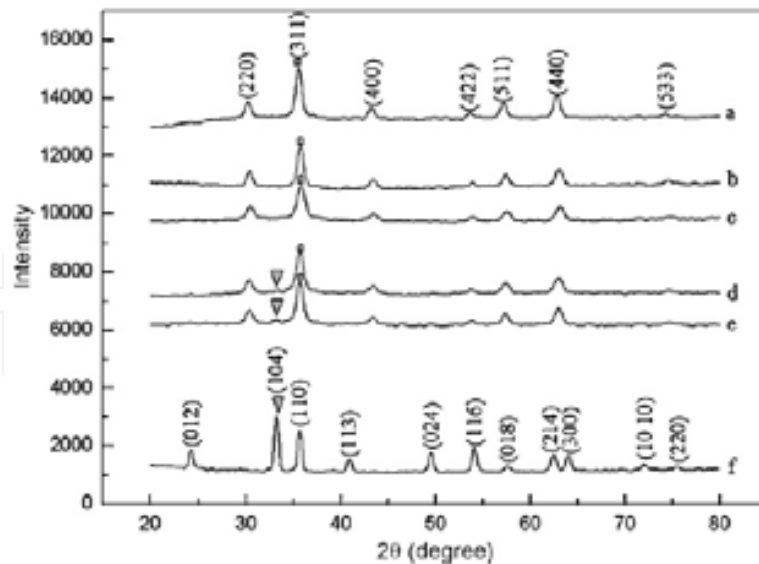


Fig. 17. XRD patterns of pure  $\text{Fe}_3\text{O}_4$  nanoparticles at room temperature (a) and calcined at  $150^\circ\text{C}$  (b),  $250^\circ\text{C}$  (c),  $350^\circ\text{C}$  (d),  $450^\circ\text{C}$  (e),  $550^\circ\text{C}$  (f) for 2 h in the atmosphere [28].

### 3.3.2 Infrared spectroscopy (IR)

From the IR spectrum, one can observe the absorption and emission due to the molecular vibration and rotation in the electromagnetic wave infrared region ( $15000\sim 10\text{ cm}^{-1}$ ). It reveals the unknown composition qualitatively according to the bands characteristic frequency, determines a component content of the sample (quantification) according to band intensity. It can also reveal the molecular structure (such as functional group, bond), identify isomer, and determine structures of compounds. The interaction among molecules can also be understood by anatomizing the band change. This method can be used to measure samples in the state of gas, liquid and solid. There are also extremely sensitive changes in molecular structure called "fingerprint zone" ( $1300\sim 400\text{ cm}^{-1}$ ), which provides a reliable determination to analyze unknown composition and structure.

Figure 3-8 shows that no change of XRD patterns can be observed for pure  $\text{Fe}_3\text{O}_4$  nanoparticles after being calcined at  $150^\circ\text{C}$  and  $250^\circ\text{C}$ . To reveal the difference, IR spectra (as shown in Fig. 18.) of magnetite samples calcined at different temperatures were obtained using FT-IR. From Fig. 18., one can find the absorption peak of Fe-O in  $\text{Fe}_3\text{O}_4$  at  $571.1\text{ cm}^{-1}$ . After calcined at  $150^\circ\text{C}$  for 2 h, the peak at  $571.1\text{ cm}^{-1}$  splits into two peaks at  $632.9$  and  $563.4\text{ cm}^{-1}$ , respectively. The new arisen absorption peaks at  $632.9$  and  $563.4\text{ cm}^{-1}$  which are associated with Fe-O bond, are the characteristic peaks of  $\gamma\text{-Fe}_2\text{O}_3$ . XRD is not sensitive enough to differentiate between  $\text{Fe}_3\text{O}_4$  and  $\gamma\text{-Fe}_2\text{O}_3$ , due to extreme similar similarity in crystal structure of the two phases. Provided that there is an intergradation, in which  $\text{Fe}_3\text{O}_4$  and  $\gamma\text{-Fe}_2\text{O}_3$  coexist at a certain proportion that owns the maximal magnetism. The intergradation appears when the pure  $\text{Fe}_3\text{O}_4$  nanoparticles were calcined at  $250^\circ\text{C}$  for 2 h in air, leading to the maximal magnetism. Afterwards, the peak at  $632.9\text{ cm}^{-1}$  becomes increasingly weaker, and disappears at  $550^\circ\text{C}$ . While, another new peak at  $447.6\text{ cm}^{-1}$  comes forth at  $450^\circ\text{C}$ , and the peak becomes stronger and shifts to  $463.1\text{ cm}^{-1}$  when at  $550^\circ\text{C}$ . According to Nasrazadani and Raman the two absorption peaks at  $532.5\text{ cm}^{-1}$  and  $463.1\text{ cm}^{-1}$  can be assigned to the Fe-O absorption in hematite ( $\alpha\text{-Fe}_2\text{O}_3$ ). Therefore, one can get that  $550^\circ\text{C}$  is the minimal temperature for the complete transformation from magnetite ( $\text{Fe}_3\text{O}_4$ ) to hematite ( $\alpha\text{-Fe}_2\text{O}_3$ ), consistent with the results of XRD and magnetic properties analysis.

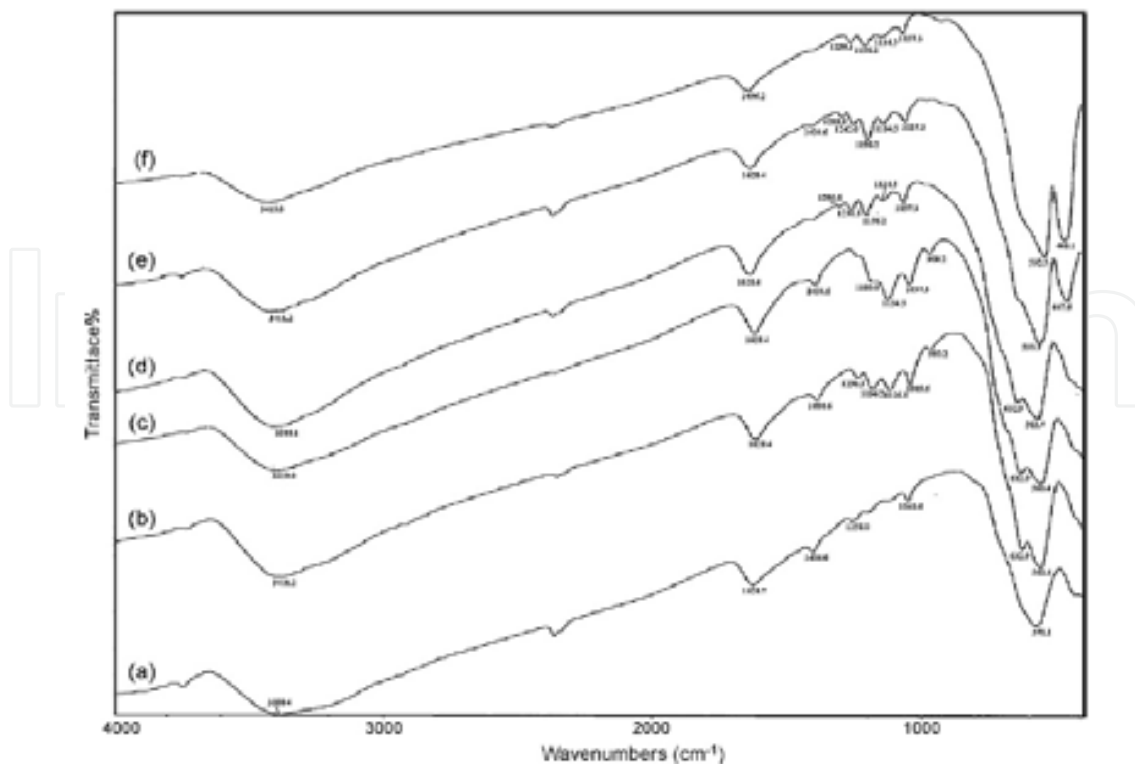


Fig. 18. IR spectra of pure  $\text{Fe}_3\text{O}_4$  nanoparticles at room temperature (a) and calcined at 150°C (b), 250°C (c), 350°C (d), 450°C (e), 550°C (f) for 2 h in the atmosphere [28].

### 3.3.3 Mechanical property test

The mechanical property of the prepared films can be measured using the universal material testing machine (WDT-0.2, KQL Testing Instruments Inc., China). The force transducer with a precision of  $\pm 0.02\%$  was made by Transcell Tech. Inc., USA. The maximum range of the transducer is 30 kg. The crosshead speed was 5 mm/min during the tests. The films were cut into dumb-bell shape and the mechanical property measurement was performed according to our previous articles.

The mechanical property of pure PU films and ZnO-doped PU films prepared using PU coatings were measured [29]. Fig. 14. shows the tensile stress-strain curves of the PU films and the mechanical parameters are listed in Table 3. It can be seen that the Young's modulus and tensile strength increase first and then decrease with the increasing ZnO content and the optimal ZnO content for the Young's modulus and tensile strength is obtained at 2.0 wt%. However, the elongation at rupture goes inversely relating to the Young's modulus and tensile strength. Repeated tests show that the filled ZnO nanoparticles can enhance the strength but not the flexibility of the composite films. The elevation of Young's modulus and tensile strength of the composite films may be due to the limit of moving scale of chain segments of the PU matrix with the addition of ZnO. Moreover, when ZnO nanoparticles are filled into the interstice of PU chains, an interactive force against the PU chains may be generated. Therefore, when an external force is applied onto the two ends of the dumb-bell-shaped PU film, the film goes to rupture easily due to the strong interaction force generated between ZnO nanoparticles and PU chains. Besides, the percolation effect could cause the aggregation of ZnO nanoparticles in the dry film, leading to the deterioration of mechanical property.

ZnO (wt%)	Young's modulus (MPa)	Tensile strength (MPa)	Elongation ratio At rupture (%)
0.0	517.42	8.58	98.37
1.0	660.34	16.74	94.35
2.0	710.48	17.83	54.79
3.0	557.70	10.42	77.96
4.0	512.76	7.24	70.69

Table 3. Mechanical property of the PU films filled with different ZnO content [29].

### 3.3.4 Abrasion resistance test

The neat PU coatings and 2.0 wt% ZnO nanoparticles filled PU coatings were sprayed onto a ABS substrate with a 1 mm×1 mm grounding area. The obtained wet coat was roasted for curing under infrared ray at 60°C for 30 min. The abrasion resistance of the selected coat was tested using a pencil-abrasion-resistance tester. In the testing process, a sample area, which was free of blemishes and painting imperfection, was selected. The eraser was kept closely contacting with the surface of the sample at 90°. The moving distance was limited to 2.54 cm, and the frequency was maintained at 25 rpm. The test was performed by moving the free end of the pencil until the grounding area, which was a useful indicator when some cracks were made, was revealed. The total times of the eraser moving back and forth indicate the abrasion resistance of the coat.

Table 4. shows the abrasion resistance of the dry and alcohol wetted PU composite coats. It demonstrates that the abrasion resistance of the composite coats is improved when ZnO nanoparticles were filled into the PU matrix. The improvement of abrasion resistance for the samples with ZnO nanoparticles may be attributed to the polymer bond formed around the hard nanoparticles. Compared with the dry coats, the wet coats demonstrate poor abrasion resistance, indicating poor endurance against organic solvent, such as alcohol. Besides, one can also see that the abrasion resistance of the dry and wet coats is linear to the thickness, and the slopes are 0.9664 (dry, neat), 0.9906 (wet, neat), 0.9910 (dry, composite) and 0.9937 (wet, composite), respectively. Moreover, the PU composite coats possessing the same abrasion resistance are much thinner than the pure PU coats, which revealing that the addition of ZnO nanoparticles, is favorable for reducing manufacturing cost and displays an outstanding prospect in application.

Thickness (µm)	Neat PU film		Composite film (2.0 wt% ZnO)	
	Dry	Wetted with alcohol	Dry	Wetted with alcohol
10	148	60	361	86
12	155	77	410	97
14	162	91	437	113
16	187	101	497	133
18	206	110	560	156

Table 4. The abrasion resistance of the composite coats with various thickness from 10 to 18 µm [23].

### 3.3.5 Impact strength

To obtain the impact strength of nanocomposites, an Izod impact machine tester with digital display (JBL-22, Shenzhen KQL Testing Instruments Co., Ltd) was used according to GB/T 1843-1996. Unnotched specimens with rectangular dimensions of  $80 \times 10 \times 4 \text{ mm}^3$  were fractured by the impact energy of 5.5 J with an impact speed of 3.5 m/s at room temperature. The distance between the impact point and fixed point was set to 22 mm.

The impact strength of PMMA nanocomposites is shown in Fig. 19. For Sample A, the filling of silica particles obviously improves the impact strength of PMMA nanocomposites. The impact strength of PMMA nanocomposites increases with the increasing silica content, which can be ascribed to the more reinforcement sites formed among the polymer chains. It suggests the importance of incorporating the silica particles to improve the mechanical properties of PMMA nanocomposites. Considering the strong increase in impact strength of PMMA nanocomposites, it is obvious that some energy is eliminated by the filled silica particles during the breaking-down process. As for Sample B, the impact strength is enhanced at low content of silica ( $x = 0.5$ ) and then weakened at high content ( $x = 1$  or 1.5). With the increasing silica content, more THF is left in the polymer composites and thereafter induces the formation of small pin-holes in PMMA during the heat treatment at  $100^\circ\text{C}$ . During the test of impact strength, such pin-holes become the weak points and the PMMA nanocomposites are easy to be broken under an abrupt impact and the impact strength decreases.

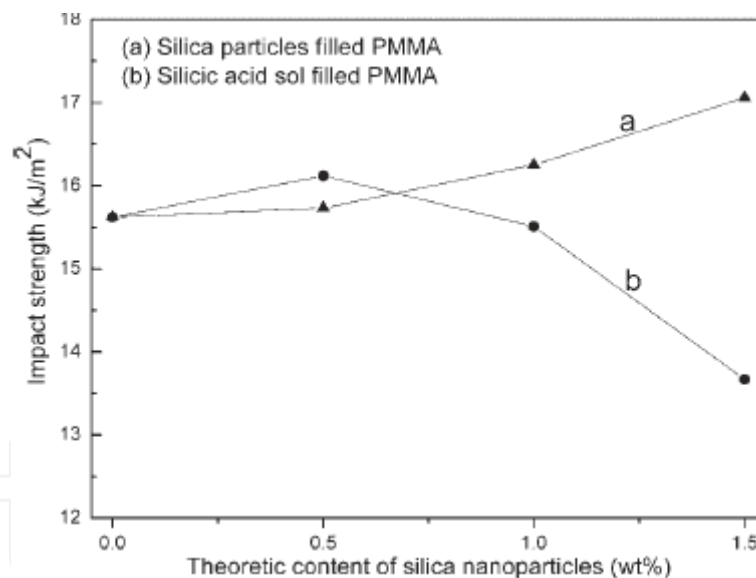


Fig. 19. Impact strength of different PMMA nanocomposites [14].

### 3.3.6 Flexural test

Flexural test could be performed according to GB/T 9341-2000<sup>26</sup> using a universal testing machine (WDT20, Shenzhen KQL Testing Instruments Co., Ltd) in a three-point bending configuration at room temperature. A PC was connected to the testing machine, and the crosshead speed was set to be 2 mm/min. Another force transducer with a maximum range of 2 ton is used. The transducer with a precision of  $\pm 0.02\%$  was made by Transcell Tech. Inc. USA. The effect of particulate fillers on the stress-strain behavior of polymeric materials can be much different due to the interaction between the particles and polymer. The flexural

strength measured for different PMMA nanocomposites is shown in Fig. 20. It can be concluded that as the silica content increases, the flexural strength of PMMA nanocomposites either filled by silica particles or by silicic acid sol increases. The reinforcement mechanism of polymer by silica can be explained as this: as the active surface of silica particles connected with some long polymer chains and the physical bonding between silica and polymer chains are formed, the flexural stress could be transferred through the inorganic linking point to the other polymer chains. When one chain gets ruptured under external stresses, the others can still support the polymer structure. So the whole specimen is not threatened by the stresses, and the flexural strength enhances. For the Sample A, as the content of silica particles increased, the number of coupling points between PMMA and silica particles also increased; therefore, the flexural strength is improved. As for Sample B, contrary to the impact strength, the flexural strength is enhanced with the addition of more silicic acid sol, though there maybe small pin-holes existing in the composites. There are two factors influencing the flexural strength of PMMA nanocomposites: the addition of silica and the existence of pin-holes in the structure. During the test, stress was imposed slowly on the samples, though the pin-holes might lower the flexural strength; however, such influence was negligible. On the contrary, the silica well dispersed in PMMA nanocomposites has an obvious enhancement to the flexural strength. As a result of the two opposite effects, the flexural strength of silicic acid sol filled PMMA nanocomposites is improved.

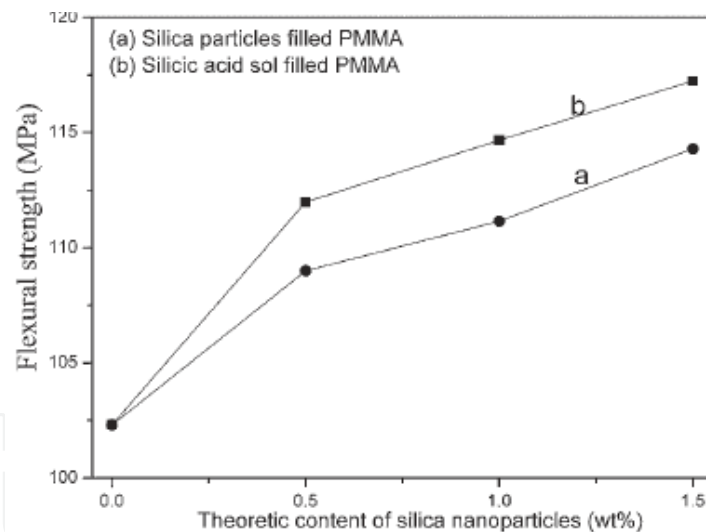


Fig. 20. Flexural strength of different PMMA nanocomposites [14].

### 3.3.7 Others

Scanning Tunneling Microscopy (STM) is a microscope based on the principles of electron tunneling. Between two closed conductors (typically only a few Å) electrons can pass through the barrier between two conductors and flows under external electric field, which calls the tunnel effect. This electrons produce measurable current, the value and the distance between the conductors has exponential relationship:  $I \propto V \exp[-C(\phi S)^{1/2}]$  where  $I$ -tunneling current,  $V$ -added voltage between conductors,  $\phi$ -effective tunneling barrier (eV),  $C$ -constant,  $S$ -2 conductor spacing (Å). STM is precise enough to control the positioning of



individual atoms on the probe, and can scan atom one by one in atomic array, which provides atomic resolution of surface analysis.

The main feature of Atomic Force Microscopy (AFM) is that it does not require the surface conductivity, because it measures the scanning probe and the interaction between the tip of AFM and the sample surface. The interreaction includes electrostatic, van der Waals, friction, surface tension (capillary) and the magnetic force, which overcomes the inadequacy of the STM. Unlike the STM, a force map can be obtained from the AFM probe. This map can be interpreted as a reflection of the surface structure and a geometric topology map of magnetic and electrostatic forces.

In addition to the above spectroscopic methods, there are still a variety of other methods, such as Mössbauer spectroscopy, surface analysis spectra and dynamic structure spectroscopy. As is well known, the surface analysis and surface characterization methods are more than 100 kinds. This shows the difficulty of surface characterization. When one characterizes the surface and its structure, it is necessary to integrate different analysis and characterization methods to complement and confirm each other.

#### **4. Application of polymer-inorganic nanocomposites**

##### **4.1 Applications of Bi-YIG films and Bi-YIG nanoparticles doped PMMA**

Bi-YIG films and Bi-YIG nanoparticles doped PMMA nanocomposites are the functional materials with magneto-optical effects from the ultraviolet to the infrared band ray. With profound investigation of Faraday rotation and gradual recognition of the importance of the effect, people began to take advantage of this effect in practical applications. Various magneto-optical devices prepared using the magneto-optical materials have been widely used in the field of optical communication and optical storage. Magneto-optical modulator, magneto-optical switcher, magneto-optical isolator, magnetic optical circulator, magneto-optical rotator and magneto-optical phase shifter have been invented since 1966.

With the development of optical fiber communication and integrated optics, the integrated magneto-optical waveguide-type device was invented in 1972. The first-generation magneto-optical disc was launched in 1988, which has many distinct advantages, such as high-density recording ( $10^7 \sim 10^{10}$  bit/cm<sup>2</sup>), erasable writing, rewritable, etc. In addition, the materials with magneto-optical effect are also widely used in the field of magnetic field measurement, high-voltage transmission lines and current measurement sensors, and magneto-optical storage. As the core material of the magneto-optical devices, magneto-optical materials determined the merits of the performance of devices directly. Magneto-optical device has high sensitivity, strong anti-interference, high insulation, low cost, small size, light weight and so on. The material is also widely used in the fields of space, guidance, and satellite monitoring and controlling. Take the advantage of the independent of the magnetic rotation direction with the incidence light direction, the materials can be made into a single-pass optical gate and modulator. The magneto-optical glass with high Verdet Constant (also known as Vd values) can be used for the measurement of high current to prevent accidents caused by lightning and short-circuit of electrical devices.

Magnetic nanoparticles with magneto-optical effect have important applications. Polymethyl methacrylate (PMMA) doped with these nanoparticles demonstrates magneto-

optical effect and can be used to prepare a variety of devices. The following are some of the mature applications.

#### 4.1.1 Magneto-optical sensor

Magneto-optic sensor is a device to take advantage of magneto-optical effects to detect the changes in magnetic field or current strength. It combines laser, optical fiber and optical techniques in one. It is widely used in high-voltage network testing, monitoring, precision measurement, remote control, telemetry and automated control systems.

The typical structure of a current sensor using optical fiber is shown in Fig. 21. The working principle is: the light sent off by a laser through the polarizer becomes linear polarized light, then the linear polarized light transmits through the optical fiber which winds around the electrical wire. As a result of the Faraday rotation, the polarization angle of linear polarized light deflects. Owing to the changes of light intensity, the analyzer detects the change of the linear polarized light intensity caused by the Faraday deflection, so the actual current can be measured. Traditionally, high-voltage measurement and monitoring used the oil-filled magnetic flux current transformer (OFMFCT). The transformer used much copper wire, insulation materials and machining parts. Compared with OFMFCT, the magneto-optical sensor has some benefits, such as a simple structure, small size and low cost. It is considered to be the most promising high-voltage and high-current measuring devices.

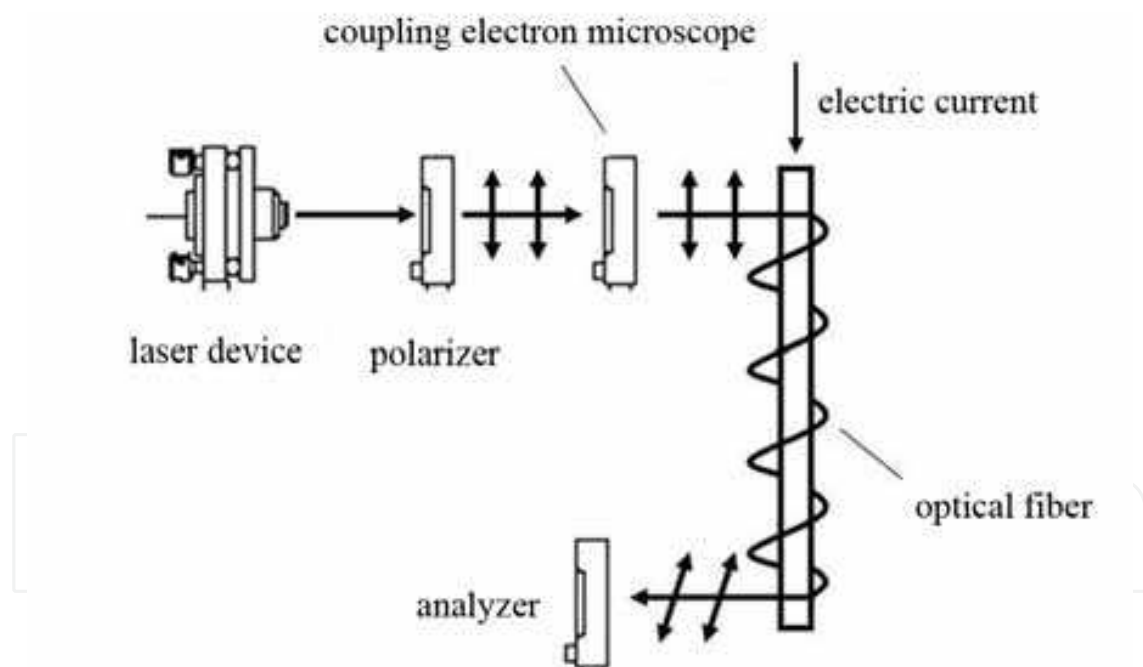


Fig. 21. The structure of a current sensor using optical fiber.

#### 4.1.2 Tuned filter

YIG tuned filter is a device for filtering. A YIG small ball, as the oscillator, selects input signal through the resonant frequency generated by coupling. It works in the frequency range of 3 ~ 40 GHz, and 3 dB bandwidth can be adjusted between 5 ~ 70 MHz. Having a very wide frequency tuning range (up to several octave), the YIG is widely used in broadband MW, millimeter-wave receiver for tracking and pre-selecting RF signals.

In the MW frequency, the YIG molecules have a magnetic moment. Normally, the moment was randomly arranged. When a static magnetic field is applied, the magnetic moment will be arranged towards a certain direction. If an alternating magnetic field is applied, the moment will change back and forth. The oscillation frequency is the function of the properties of YIG materials (e.g., magnetic properties, crystal shape and size), and the intensity of magnetic field. The maximum amplitude that appears in alternating magnetic fields exactly equals to the oscillation frequency of YIG crystal. Therefore, we can take advantage of this resonance phenomenon to create filters, as shown in Fig. 22.

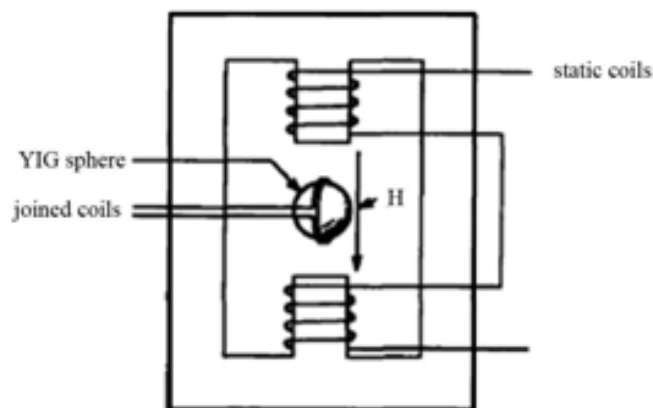


Fig. 22. The using of resonance phenomenon to create filters.

A typical YIG resonator constitutes a highly polished YIG sphere with a diameter of 0.25 ~ 0.5 mm. A small ball is put in the static magnetic field with the field strength of  $H$ . When a signal enters the input side, the ball produces a circular polarized magnetic moment around the small ball if the signal frequency is equal to the resonant frequency of resonator. When the magnetic field couples with the output coil, the energy generates from the output coil. Otherwise, the small ball is not inspired and no energy is generated.

#### 4.1.3 Magneto-optical recorder

The principle of magneto-optical recording was proposed early in the nineteen fifties, but its specific application was developed in recent years. Magneto-optical recording is the most advanced information storage technology, which combines the advantages of both magnetic disk and CD-ROM. Magnetic discs are widely used in many applications that require large-scale real-time data collection, recording, storage and analysis. The magneto-optical storage systems will replace the traditional storage methods.

Magneto-optical recording technology stores information by heating the small magnetic area to change the orientation of magnetization vector, and then reads out the information using magneto-optical effects. In practical application, the thin and amorphous film placed in reverse magnetic field was heated by a laser beam, resulting in magnetization perpendicular to the membrane surface. Information can be written onto the magnetic domain, and read out by magneto-optic Kerr effect. The most important characteristics of the magneto-optical recording material is that magnetic recording medium should be perpendicular to the membrane surface, and can maintain the stable structure of the small magnetic domain. The magneto-optical Kerr rotation angle of the materials must be large, and reflectivity must be high to enough to achieve high sensitivity and low noise. Moreover, the chemical structure must be stable, and the large film can easily be produced.

A practical magneto-optical recording medium must have the following features: the magnetic anisotropy perpendicular to the membrane surface, and the  $K_u > 2\pi M_s^2$ ; a rectangular hysteresis loop ( $M_r/M_s=1$ ) and high coercivity at room temperature; high magneto-optical recording sensitivity (lower laser recording power); large magneto-optical effect (a large Kerr angle  $\theta_k$  or large Faraday angle  $\theta_F$ ); low disk writing noise (no big grain); high enough reading and writing cycles; good oxidation resistance, corrosion resistance and long-term stability; Curie temperature between 400 ~ 600 K and compensation temperature at 25°C. In the last two decades, a new magneto-optical material through the replacement of old ones, the current rare-earth transition metal (RE-TM) materials, magneto-optical disc has been put into the market. However, owing to its weak magneto-optical effect, chemically unstable, high price, as well as poor magneto-optical effects near ultraviolet, people began to explore the next generation materials. Bi, Ga substituted Yttrium Iron Garnet magneto-optical material as a new generation of magneto-optical materials has been researched and developed.

#### 4.1.4 Magneto-optic modulator

Magneto-optic modulator modulates light beam by rotating the polarization plane of the incidence light through the magneto-optical medium. The modulator has a wide range of applications, e.g., infrared detectors chopper, infrared radiation pyrometer, TV signal transmission and distance measuring devices, optical detection and transmission system.

The structure and working principle of magneto-optical modulator is illustrated in Fig. 23.



Fig. 23. The structure and working principle of magneto-optical modulator.

There is no external magnetic field in the absence of modulated signals. When a beam of intensity  $I_0$  goes through the polarizer, the output intensity is as follows according to Malus law:

$$I = I_0 \cos^2 \alpha$$

where  $a$  is the angle between the optical axis of polarizer and the analyzer. When the two optical axis is parallel ( $a = 0$ ), the light intensity  $I$  is maximum. When the two polarizers is perpendicular to the beam ( $a = \pi/2$ ), the light intensity  $I$  is zero (the output is extinct). When the alternating signal is applied on the electrical coils of magneto-optical materials, an alternating magnetic field is generated and the polarization plane of light is thus rotated. The output light intensity is as follows:

$$I = I_0 \cos^2(\alpha \pm \theta)$$

when  $a$  is constant, the output light intensity is only changed with  $\theta$ . Due to the Faraday rotation effect, the signal current modulates the rotation signal of polarized light into intensity signal. Modulation information was carried by the output light in the form of intensity changing.

During the production of magneto-optic modulators, it requires that the magneto-optical materials should have high transparency and large Faraday rotation (Faraday rotation angle per unit length). The magneto-optical glass was previously used. Currently, the YIG was invented, which has high transparency and high Faraday rotation angle in the  $1.1 \sim 5.5 \mu\text{m}$  wavelength. As the single-crystal epitaxial thin film magneto-optical material, the Bi-doped YIG is more suitable for preparing the optical modulator. The Faraday rotation angle of the device is as high as  $10^3 \sim 10^4 \text{ rad/cm}$ , while the transparency to visible light is still high. For more applications of Bi-YIG, please read section 3 of our recent book [30].

#### 4.2 Application of magnetic $\text{Fe}_3\text{O}_4$ based nanocomposites

With the development of industry, waste water from many industries such as chemical manufacturing, mining, battery manufacturing industries, etc., contains toxic heavy metals, which are not biodegradable, causing various diseases. For instances, chromium is present in effluent waters from several different industries. It affects human health, accumulates in the food chain and causes many ailments. Contact with chromium results in severe health problems such as simple skin irritation and lung carcinoma [31]. Strong exposure to Cr(VI) could cause cancer in the digestive tract and lungs, epigastric pain and nausea. Copper is the most important and frequently used metal in industries such as plating and petroleum refining. The industries mentioned above produce much wastewater and sludge containing a high concentration of copper cations, which have negative effects on the environment [32]. The problems of Cadmium and the solutions of its compounds have been found from long-term exposure and work with cadmium plating baths. Uniformity, nickel sulfide fume is recognized as a carcinogenic material. At the same time, the requirement of Ni-Cd batteries has been growing visibly in recent years. It means that there will be enhanced potential for an increasing content of Ni and/or Cd in water. Hence, it is very important to purify water before being used as it is one of the basic demands for the survival of human. And the effective disposal of heavy metals has aroused worldwide concern in the last few decades.

Nowadays, various treatment techniques have been used to remove the metallic ions from the wastewater, such as precipitation, evaporation, solvent extraction, ion exchange, reverse osmosis, membrane separation. Most of these methods suffer from some drawbacks such as high capital and operational costs for the treatment and disposal of the residual metal sludge [33-35]. Therefore, great efforts are taken to develop low-cost materials for removing contaminants from aqueous solutions. Thankfully, recent development of nano-technique has made great progress on this field. Nanoparticles, characterized by a significant amount

of surfaces, have got a great deal of attention, because of their unique properties and potential applications.

For an instance, magnetic  $\text{Fe}_3\text{O}_4$  nanoparticles have attracted much attention not only in the field of magnetic recording but also in the areas of medical care and magnetic sensing [36-38]. It is believed that magnetic nanoparticles exhibit the finite-size effect or high ratio of surface-to-volume, resulting in a higher adsorption capacity for metal removal. In addition, the easy separation of metal loaded magnetic adsorbent from solution can be achieved using an external magnetic field. Thus, an efficient, economic, scalable and non-toxic synthesis of  $\text{Fe}_3\text{O}_4$  nanoparticles is highly preferred for potential applications and fundamental research [39-41].

Several recent studies sought to adsorb heavy metals onto magnetic nanoparticles. For example, the removal and recovery of Cr(VI) has been achieved by synthesized maghemite ( $\gamma\text{-Fe}_2\text{O}_3$ ) nanoparticles, and it is proved that Cr(VI) adsorption capacity of nanoscale maghemite compared favorably with other adsorbents like activated carbon and clay [42,43]. Very interestingly, a further study from the same group suggests that the Cr(VI) adsorption onto the  $\delta\text{-FeOOH}$ -coated  $\gamma\text{-Fe}_2\text{O}_3$  is mainly controlled by the outer-sphere complexation [44]. They also proved that the Cr(VI) can be effectively removed from synthetic wastewater using surface modified jacobite nanoparticles, in which the adsorption process followed by magnetic separation leads to the rapid, effective and inexpensive removal of toxic ions [45]. The results from another group have shown that magnetic nanostructured particles  $\gamma\text{-Fe}_3\text{O}_4$  can be successfully applied to adsorb metal ions, in which the combined technique of biosorption and magnetic separation holds the advantages of flexibility, eco-friendly characteristics and economic in operational cost [46]. Recently, a successful removal of Cr(VI) has been achieved by electro-coagulation with Fe electrodes [48]. Of course, there are many other applications, such as protein separation and cell separation.

For more applications, please read section 7 of our recent book [47].

### 4.3 Application of ZnO based nanocomposites

Nanosized ZnO has a bright future for being used in preparing solar cell, gas sensors, chemical absorbent varistors, electrical and optical devices, electrostatic dissipative coating, catalysts for liquid phase hydrogenation, and catalysts for photo-catalytic degradation instead of titania nanoparticles. Hence, investigations on the synthesis and modification of nanosized ZnO have attracted tremendous attentions.

#### 4.3.1 Gas sensing materials

ZnO has high chemical stability, low dielectric constant, large electromechanical coupling coefficient, ZnO materials have been widely used as dielectric ceramic, pigment, catalyst and sensing material [48]. As a gas sensing materials [49], it is one of the earliest discovered and the most widely applied oxide gas sensing material. It is sensitive to many kinds of gases, and has satisfactory stability. Its gas selectivity can be improved by doping additives and catalysts. But its working temperature is rather high, normally 400-500°C, and its gas selectivity is poor. In recent years, the studies on ZnO gas sensing materials, which can improve its preparation method and decrease its working temperature, are one of its major research topics [50].

#### 4.3.2 Photocatalyst for degradation of organic dye

The use of semiconductor colloids as photocatalyst for a variety of chemical reactions, due to their peculiar optoelectronic photocatalytic properties, is well stated in the recent literatures

[51-53]. The effectiveness of the photodegradation processes has already been tested for different types of matrices and results have been encouraging, as the literature reports on a large number of successes in the degrading of organic dyes in waste water [54]. Under photo-excitation semiconductors undergo charge separation and initiate oxidation of the organic compounds at the interface. Nanostructured semiconductors are a potential candidate to photodegradation of organic compounds because of the size-dependence of their band gap [55], when the semiconductor nanocrystal size is comparable or smaller than the bulk exciton diameter. Therefore, photocatalytic electron and hole redox potentials of size quantized semiconductor nanocrystals can be tuned to achieve increased catalytic effect for selective photochemical reaction. Moreover, as photocatalytic reaction occurs at nanoparticles surface, nanosized semiconductor high surface to volume ratio will contribute to increase the decomposition rate.

Synthetic routes using the principles of colloidal chemistry provide the possibility of separate nucleation from growth, avoiding particles aggregation and controlling their growth. In this paper, nanostructured TiO<sub>2</sub> and ZnO were prepared using new non-hydrolytic methods [56]. These preparative approaches are based on the rapid thermal decomposition of molecular precursors in the presence of strong coordinating agents to produce high crystalline, redispersible, nanosized semiconductor particles, with controllable size and size-distribution. The reactions occur at high temperatures in anhydrous organic solvents, providing oxide nanoparticles with no surface hydroxyl groups, which are known to significantly influence surface oxidation power as well as to decrease interfacial electron-transfer rates with respect to their dehydroxylated counterparts. After optical and structural characterization, the obtained nanoparticles were immobilized onto transparent support in order to exploit them in a photocatalytic process devoted to the photodegradation of methyl red, an organic dye. Then a comparison between the efficiency of nanocatalysts and their equivalent commercial oxides were performed. The obtained results showed a high efficiency.

#### 4.4 Application of magnetic fluid

Magnetic fluids, which are colloidal suspensions of magnetic nanoparticles stabilized by coating surfactants, have attracted much interest recently. Magnetic fluids have been widely used in loudspeakers, hard discs, dynamic sealing, electronic packing, mechanical engineering, aerospace, bioengineering, biological and medical diagnosis and therapy, pharmacy and biosensors.

Sealing techniques of magnetic fluid take advantage of the response of magnetic fluid in a magnetic field. When a magnetic fluid is placed into a gap between the surfaces of rotating and stationary elements in the presence of magnetic field, it assumes the shape of a "liquid O-ring" to completely fill the gap.

The magnetic fluid vacuum rotary feed through is a device that transmits rotary motion into a vacuum chamber. The basic components are permanent magnet, two pole pieces, a magnetically permeable shaft and magnetic fluid. The shaft (of pole pieces) contains a multistage structure, completed by the pole pieces and the shaft, concentrating magnetic flux in the radial gap under each stage. In the ideal situation, all flux lines are confined under each stage, and none are in increase region. The magnetic fluid is trapped and held in each stage, forming a series of "liquid O-ring" with intervening regions that are filled with air. Each stage can typically sustain a pressure differential of 0.15 - 0.2 atmosphere. All stages act in series to provide a total pressure capability for the seal. For vacuum applications, magnetic fluid seals are normally designed to sustain a pressure differential of greater than two atmospheres, thus allowing a safety margin.

In our researches, biocompatible magnetic fluids based on dextran-coated  $\text{Fe}_3\text{O}_4$  magnetic nanoparticles was prepared through a one-step method [57]. In contrast to the conventional co-precipitation method, hydrazine hydrate was added as reducing agent and precipitator in the present investigation. The prepared biocompatible magnetic fluids was intravenously injected into rabbits, the iron content in blood and organs at different times were measured by atomic absorption spectrometer, and the bio-distribution and the bio-transportation of magnetic fluids in organs was examined. Then, the magnetic resonance (MR) images of liver, marrow and lymph (as shown in Fig. 24.) were acquired by MRI experiments before and after intravenous injection of magnetic fluids. Image analysis revealed that the MR signal intensity of these organs notably decreased after being intensified by magnetic fluids. However, when there existed tumors in organs, the signal intensity of tumor did not change after injection. From that the tumor can easily be identified, which indicated a potential application of the as-prepared magnetic fluids in functional molecular imaging for biomedical research and clinical diagnosis.

t(h)	Blood (mg/g)	Lymph (mg/g)	Liver (mg/g)	Spleen (mg/g)	Lung (mg/g)	Heart (mg/g)
0	0.048	0.010	0.079	0.297	0.038	0.042
0.5	0.255	0.019	0.08	0.316	0.056	0.047
1	0.275	0.02	0.23	0.931	0.093	0.056
2	0.256	0.053	0.188	1.028	0.137	0.095
3	0.14	0.154	0.169	0.656	0.152	0.091
6	0.105	0.206	0.14	0.652	0.097	0.072
9	0.081	0.073	0.113	0.598	0.061	0.071
12	0.050	0.07	0.106	0.594	0.042	0.063

Table 5. The Fe contents in some organs of rabbits at different times [23].

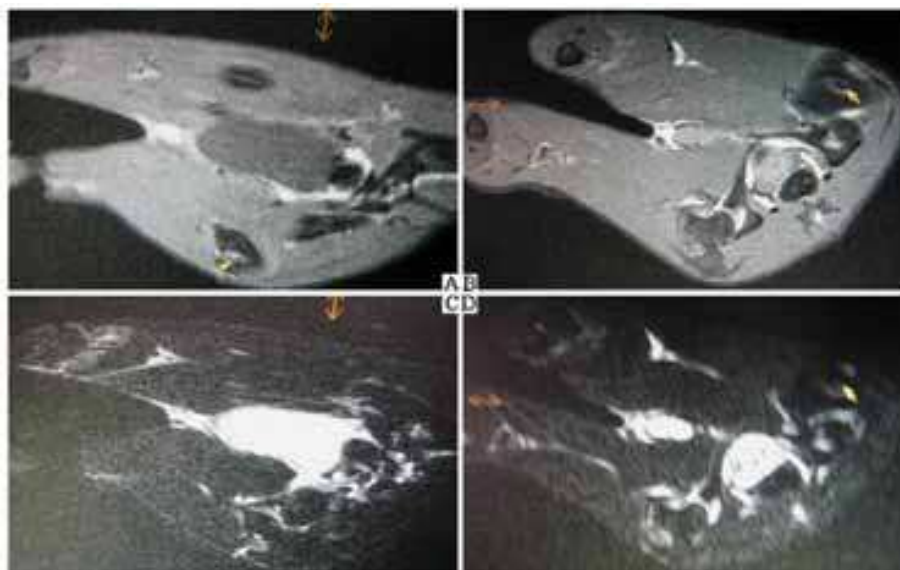


Fig. 24. MR signals intensity of lymph of rabbit in T1-weighted sequences (A and B) and T2-weighted sequences (C and D). Images were acquired before (A and C) and 6 h after intravenous injection of  $\text{Fe}_3\text{O}_4$  MNPs (B and D) [58].



For more application of magnetic fluid in industry, biotech and pharmaceutical fields, please read section 7 of our recent book [47].

## 5. Acknowledgments

The project was supported by the National Natural Science Foundation of China (NSFC, Nos. 20876100 and 20736004), the National Basic Research Program of China (973 Program, No. 2009CB219904), the State Key Lab. of Multiphase Complex Systems of the Chinese Academy of Science (No. 2006-5), the Key Lab. of Organic Synthesis of Jiangsu Prov., R&D Foundation of Nanjing Medical Univ. (NY0586), Post-doctoral Science Foundation of Jiangsu Prov., National Post-doctoral Science Foundation (20090451176), the Commission of Science and Technology of Suzhou Municipality (YJS0917, SG0978), Technology Innovation Foundation of Suzhou National Hi-Tech District and MOST, and Minjiang Scholarship of Fujian Prov.

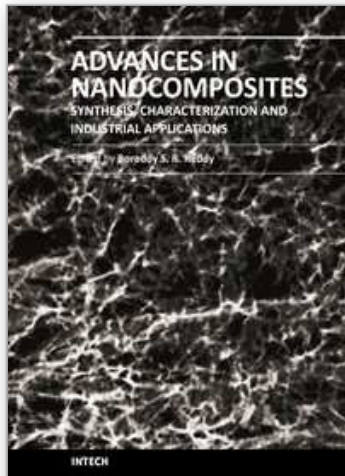
## 6. References

- [1] R.Y. Hong, Z.Q. Ren, J.M. Ding, H.Z. Li, *Chem. Eng. J.*, 108 (2005) 203-212.
- [2] R.Y. Hong, T.T. Pan, H.Z. Li, *J. Magn. Magn. Mater.*, 303 (2006) 60-68.
- [3] R.Y. Hong, J.H. Li, J. Wang, H.Z. Li, *Particuol.* 5 (2007) 186-191.
- [4] R.Y. Hong, T.T. Pan, Y.P. Han, H.Z. Li, J. Ding, S.J. Han, *J. Magn. Magn. Mater.*, 310 (2007) 37-47.
- [5] R.Y. Hong, J.H. Li, H.Z. Li, J. Ding, Y. Zheng, D.G. Wei, *J. Magn. Magn. Mater.*, 320 (2008) 1605-1614.
- [6] R.Y. Hong, T.T. Pan, J.Z. Qian, H.Z. Li, *Chem. Engin. J.*, 119 (2006) 71-81.
- [7] R.Y. Hong, J.H. Li, L.L. Chen, D.Q. Liu, H.Z. Li, Y. Zheng, J. Ding, *Powder Technol.*, 189 (2009) 426-432.
- [8] X. Cai, R.Y. Hong, L.S.Wang, X.Y.Wang, H.Z. Li, Y. Zheng, D.G.Wei, *Chem. Eng. J.* 151 (2009) 380-386.
- [9] R.Y. Hong, Y.J. Wu, B. Feng, G.Q. Di, H.Z. Li, B. Xu, Y. Zheng, D.G. Wei, *J. Magn. Magn. Mater.* 321 (2009) 1106-1110.
- [10] H.P. Fu, R.Y. Hong, Y.J. Wu, G.Q. Di, B. Xu, Y. Zheng, D.G. Wei, *J. Magn. Magn. Mater.*, 320(2008) 2584-2590.
- [11] Y.J. Wu, R.Y. Hong, L.S.Wang, G.Q. Di, H.Z. Li, B. Xu, Y. Zheng, D.G.Wei, *J. Alloys Comp.*, 481 (2009) 96-99.
- [12] R.Y. Hong, J.Z. Qian, J.X. Cao, *Powder Technol.* 163 (2006) 160-168.
- [13] R. Y. Hong, T. T. Pan, Y. P. Han, S. Z. Zhang, H. Z. Li, J. Ding, *J. Appl. Polym. Sci.*, 106 (2007) 1439-1447.
- [14] H. P. Fu, R.Y. Hong, Y. J. Zhang, H. Z. Li, B. Xu, Y. Zheng, D. G. Wei, *Polym. Adv. Technol.*, 19 (2008) 1-8.
- [15] R.Y. Hong, S.Z. Zhang, Y.P. Han, H.Z. Li, J. Ding, Y. Zheng, *Powder Technol.*, 170 (2006) 1-11.
- [16] R.Y. Hong, J.H. Li, J.M. Qu, L.L. Chen, H.Z. Li, *Chem. Engin. J.*, 1150 (2009) 572-580.
- [17] B. Feng, R.Y. Hong, L.S.Wang, L. Guo, H.Z. Li, J. Ding, Y. Zheng, D.G.Wei, *Colloids Surf. A: Physicochem. Eng. Aspects* 328 (2008) 52-59.
- [18] R.Y. Hong, B. Feng, Z.Q. Ren, B. Xu, H.Z. Li, Y. Zheng, D.G.Wei, *Chem. Eng. J.*, 144 (2008) 329-335.

- [19] R.Y. Hong, Z.Q. Ren, Y.P. Han, H.Z. Li, Y. Zheng, J. Ding, *Chem. Eng. Sci.*, 62 (2007) 5912-5924.
- [20] R. Y. Hong, H. P. Fu, Y. J. Zhang, L. Liu, J. Wang, H. Z. Li, Y. Zheng, *J. Appl. Polym. Sci.*, 105 (2007) 2176-2184.
- [21] T. Zhu, Y.J. Wu, F. Zhou, J.P. Zhu, Z.S. Chen. *J. Guizhou Univer. Technol. (Nat. Sci. Ed.)*. 37(2008)17-23.
- [22] H.P. Fu, R.Y. Hong, Y.J. Zhang, H. Z. Li, B. Xu, Y. Zheng and D. G. Wei, *Polym. Adv. Technol.*, 2008 (19) 1-8.
- [23] B. Feng, R.Y. Hong, Y.J.Wu, G.H. Liu, L.H. Zhong, Y. Zheng, J.M. Ding, D.G.Wei, *J. Alloys Comp.*, 473 (2009) 356-362.
- [24] J.H. Li, R.Y. Hong, M.Y. Li, H.Z. Li, Y. Zheng, J. Ding, *Prog. Organic Coatings* 64 (2009) 504-509.
- [25] ] H.P. Fu , R.Y. Hong , Y.J. Wu , G.Q. Di , B. Xu, Y. Zheng , D.G. Wei, *Journal of Magnetism and Magnetic Materials*, 320 (2008) 2584-2590.
- [26] R.Y. Hong, B. Feng, G. Liu, S. Wang, H.Z. Li, J.M. Ding, Y. Zheng, D.G. Wei, *J. Alloys Comp.*, 476 (2009) 612-618.
- [27] J.H. Li, R.Y. Hong, Z.X. Chen, H.Z. Li, *New Chem. Mater.*, 37 (2009) 31-33 (in Chinese).
- [28] J.H. Li, R.Y. Hong, H.Z. Li, Y. Zheng, J. Ding, D.G.Wei, *Mater. Chem. Phys.*,113(2009) 140-144.
- [29] J.Q. Hu, J.H. Li, R.Y. Hong, *Shanghai Coatings*, 46 (2007) 8-12.
- [30] R.Y. Hong, Y.M. Wang, L.S. Wang, Y.J. Wu and H.Z. Li, 2010, Bismuth-substituted yttrium iron Garnet nanoparticles: preparation and applications, in: "Yttrium: Compounds, Production and Applications", P. Lauren (ed.) Nova Science Publishers, Inc., Hauppauge, NY 11788.
- [31] F. Rozada, M. Otero, A. Morán, A.I. García, *Bioresour. Technol.*, 99 (2008) 6332-6338.
- [32] V.K. Gupta, A.K. Shrivastava, J. Neeraj, *Water Res.*, 35 (2001) 4079-4085.
- [33] M.K. Jha, V. Kumar, L. Maharaj, R. Singh, *J. Ind. Eng. Chem. Res.*, 43 (2004) 1284-1295.
- [34] S.E. Kentish, G.W. Stevens, *J. Chem. Eng.*, 84 (2001) 149-159.
- [35] M.K. Jha, R.R. Upadhyay, J.C. Lee, V. Kumar, *Desalination* 228 (2008) 97-107.
- [36] S.H. Sun, C.B. Murray, D.Weller, L. Folks, A. Moser, *Science* 287 (2000) 1989-1992.
- [37] J. Xie, C. Xu, N. Kohler, Y. Hou, S.H. Sun, *Adv. Mater.*, 19 (2007) 3163-3166.
- [38] Q.A. Pankhurst, J. Connolly, S.K. Jones, J. Dobson, *J. Phys. D Appl. Phys.*, 36 (2003) R167-R181.
- [39] S.H. Sun, H. Zeng, *J. Am.Chem. Soc.*, 124 (2002) 8204-8205.
- [40] S. Si, A. Kotal, T.K. Mandal, S. Giri, H. Nakamura, T. Kohara, *Chem. Mater.*, 16 (2004) 3489-3496.
- [41] S.R.Wan, J.S. Huang, H.S. Yan, K.L. Liu, *J. Mater. Chem.* 16 (2006) 298-303.
- [42] J. Hu, G.H. Chen, M.C. Lo-Irene, *Water Res.*, 39 (2005) 4528-4536.
- [43] J. Hu, M.C. Lo-Irene, G.H. Chen, *Sep. Purif. Technol.*, 56 (2007) 249-256.
- [44] J. Hu, M.C. Lo-Irene, G.H. Chen, *Sep. Purif. Technol.*, 58 (2007) 76-82.
- [45] J. Hu, M.C. Lo-Irene, G.H. Chen, *Langmuir* 21 (2005) 11173-11179.
- [46] H.D. Li, Z. Li, T. Liu, X. Xiao, Z.H. Peng, L. Deng, *Bioresour. Technol.*, 99 (2008) 6271-6279.
- [47] R. Y. Hong, 2009, *Magnetic nanoparticles and magnetic fluid: preparation and application*, Chem. Ind. Press, Beijing, China, ISBN 978-7-122-03772-5 (in Chinese).
- [48] X. Lou, *J. Sens. Trans. Technol.*, 3 (1991) 1-5.

- [49] T. Seiyama, A. Kato, *Anal. Chem.*, 34 (1962) 1502-1503.
- [50] S. Pan, S. Mei, *J. Sens. Trans. Technol.*, 3 (1993) 18-20.
- [51] K. Vinogdopal, P.V. Kamat, *Environ. Sci. Technol.* 29 (1995) 841-845.
- [52] M. Muneer, R. Philip, S. Das, *Res. Chem. Intermed.* 23 (1997) 233-237.
- [53] W.Z. Tang, Z. Zhang, H. An, M.O. Quintana, D.F. Torres, *Environ. Technol.* 18 (1997) 112-117.
- [54] L. Zang, C.Y. Liu, X.M. Ren, *J. Chem. Soc., Faraday Trans.* 91 (5) (1995) 917-922.
- [55] H. Al\_Ekabi, N. Serpone, E. Pelizzetti, C. Minero, M.A. Fox, R.B. Draper, *Langmuir* 5 (1989) 250-257.
- [56] A. Hagfeldt, M. Gratzel, *Chem. Rev.* 95 (1995) 49-56.
- [57] M. Kitano, T. Hamabe, S. Maeda and T. Okabe, *J. Cryst. Growth*, 102 (1990) 965-973.
- [58] R.Y. Hong, B. Feng, L.L. Chen, G.H. Liu, H.Z. Li, Y. Zheng, D.G. Wei, *Biochem. Engin. J.*, 42 (2008) 290-300.

IntechOpen



## **Advances in Nanocomposites - Synthesis, Characterization and Industrial Applications**

Edited by Dr. Boreddy Reddy

ISBN 978-953-307-165-7

Hard cover, 966 pages

**Publisher** InTech

**Published online** 19, April, 2011

**Published in print edition** April, 2011

Advances in Nanocomposites - Synthesis, Characterization and Industrial Applications was conceived as a comprehensive reference volume on various aspects of functional nanocomposites for engineering technologies. The term functional nanocomposites signifies a wide area of polymer/material science and engineering, involving the design, synthesis and study of nanocomposites of increasing structural sophistication and complexity useful for a wide range of chemical, physicochemical and biological/biomedical processes. "Emerging technologies" are also broadly understood to include new technological developments, beginning at the forefront of conventional industrial practices and extending into anticipated and speculative industries of the future. The scope of the present book on nanocomposites and applications extends far beyond emerging technologies. This book presents 40 chapters organized in four parts systematically providing a wealth of new ideas in design, synthesis and study of sophisticated nanocomposite structures.

### **How to reference**

In order to correctly reference this scholarly work, feel free to copy and paste the following:

L.S. Wang and R.Y. Hong (2011). Synthesis, Surface Modification and Characterisation of Nanoparticles, Advances in Nanocomposites - Synthesis, Characterization and Industrial Applications, Dr. Boreddy Reddy (Ed.), ISBN: 978-953-307-165-7, InTech, Available from: <http://www.intechopen.com/books/advances-in-nanocomposites-synthesis-characterization-and-industrial-applications/synthesis-surface-modification-and-characterisation-of-nanoparticles>

**INTECH**  
open science | open minds

### **InTech Europe**

University Campus STeP Ri  
Slavka Krautzeka 83/A  
51000 Rijeka, Croatia  
Phone: +385 (51) 770 447  
Fax: +385 (51) 686 166  
[www.intechopen.com](http://www.intechopen.com)

### **InTech China**

Unit 405, Office Block, Hotel Equatorial Shanghai  
No.65, Yan An Road (West), Shanghai, 200040, China  
中国上海市延安西路65号上海国际贵都大饭店办公楼405单元  
Phone: +86-21-62489820  
Fax: +86-21-62489821

© 2011 The Author(s). Licensee IntechOpen. This chapter is distributed under the terms of the [Creative Commons Attribution-NonCommercial-ShareAlike-3.0 License](#), which permits use, distribution and reproduction for non-commercial purposes, provided the original is properly cited and derivative works building on this content are distributed under the same license.

IntechOpen

IntechOpen